Journal of Wind Engineering & Industrial Aerodynamics 240 (2023) 105498

Contents lists available at ScienceDirect

Journal of Wind Engineering & Industrial Aerodynamics

journal homepage: www.elsevier.com/locate/jweia

State augmentation method for buffeting responses of wind-sensitive structures in wind environments with large turbulence intensity

Liutian Zhang [a,b], Wei Cui [a,b,c,*], Lin Zhao [a,b,c,d], Yaojun Ge [a,b,c]

[a] State Key Lab of Disaster Reduction in Civil Engineering, Tongji University, Shanghai 200092, China
[b] Department of Bridge Engineering, College of Civil Engineering, Tongji University, Shanghai 200092, China
[c] Key Laboratory of Transport Industry of Wind Resistant Technology for Bridge Structures, Tongji University, Shanghai 200092, China
[d] State Key Laboratory of Mountain Bridge and Tunnel Engineering, Chongqing Jiaotong University, Chongqing, 400074, China

ARTICLE INFO

Keywords:
Buffeting responses
Velocity quadratic terms
Extreme responses
State augmentation method

ABSTRACT

Recent studies have shown that wind fields with large turbulence intensity are frequently observed in non-synoptic winds such as typhoons and hurricanes. The quadratic terms of the fluctuating wind speed are important for calculating buffeting responses of wind-sensitive structures under high turbulence. In this study, a moment-based method, which is called the state augmentation method, is used to obtain high-order response moments and avoid the large computational cost of the high-order frequency domain method. First, the buffeting force formula with nonlinear velocity terms is established, and the Non-Gaussian buffeting force is further approximated as a polynomial of the Ornstein–Uhlenbeck (OU) process. Then, an augmented state vector is introduced to express the relationship between the statistical moments of each order, and the 1st to 4th response moments can be solved sequentially by a particular set of linear equations. Finally, the extreme responses of a single-degree-of-freedom (SDOF) tower and a long-span suspension bridge are calculated as engineering examples. By comparing the computation results with the frequency method, it is proven that this moment-based method has a sufficient accuracy in analysing quadratic terms. The calculation results also show that quadratic terms under high turbulence significantly amplify the non-Gaussian peak factor and extreme responses.

1. Introduction

Buffeting vibration is a common wind-induced vibration problem in wind-sensitive structures such as long-span bridges and high-rise buildings. For long-span bridges, although buffeting vibration does not cause dangerous aerodynamic instability such as flutter, excessive buffeting responses will cause discomfort to pedestrians and even threaten traffic safety. As early as the 1960s, Davenport applied stochastic vibration theory to bridge buffeting analysis, and established the frequency domain method of bridge structures under random wind loads (Davenport, 1962), which is known as the Davenport wind loading chain. Subsequently, Scanlan introduced the self-excited force into buffeting analysis, and considered that aerodynamic damping and stiffness are very important for the calculation of buffeting responses (Scanlan and Jones, 1990). The multimodal coupling effect has been considered in the classical frequency domain method of bridge buffeting response (Jain et al., 1996). Despite the use of different buffeting force models, the above frequency domain analysis model is also widely used in the extreme value analysis of high-rise buildings (Cui and Caracoglia, 2015, 2018) or other wind-sensitive structures (Amirinia and Jung, 2017; Azzi et al., 2021).

In the commonly used buffeting response prediction framework, the wind-induced force is seen as a Gaussian process. In the quasi-steady wind model, fluctuating velocities obey a Gaussian process, and the quadratic terms of fluctuating wind are usually ignored based on the assumption of moderate levels of wind turbulence intensity (Kareem et al., 1998). However, with the development of high-frequency wind field monitoring technology, field measurements have found that wind fields with high turbulence intensity (Liu et al., 2021; Fenerci and Oiseth, 2018) or non-Gaussian turbulence (Cao et al., 2009; Li et al., 2015) often appear in typhoons, hurricanes and other non-synoptic wind environments. Under this condition, it is more reasonable to describe the wind load by non-Gaussian stochastic process. The aforementioned frequency domain analysis may underestimate the extreme values of buffeting responses since response spectra can only describe all the statistical information of the Gaussian process (Soize, 1978; Benfratello et al., 1996; Gong and Chen, 2014).

* Correspondence to: 320 Wind Engineering Building, Tongji University, 1239 Siping Road, Shanghai, 200092, China.
E-mail addresses: 2132614@tongji.edu.cn (L. Zhang), cuiwei@tongji.edu.cn (W. Cui), zhaolin@tongji.edu.cn (L. Zhao).

https://doi.org/10.1016/j.jweia.2023.105498
Received 20 November 2022; Received in revised form 27 June 2023; Accepted 29 June 2023
Available online 13 July 2023

Nomenclature

$\boldsymbol{A}_1$, $\boldsymbol{A}_2$, $\boldsymbol{A}_3$, $\boldsymbol{A}_{i+3}$	Frequency-independent flutter derivatives
$\boldsymbol{A}_{q,i}$	Generalized frequency-independent flutter derivatives
$\overline{\boldsymbol{C}}$	Net damping matrix
$\overline{\boldsymbol{C}}_q$	Net generalized damping matrix
$\boldsymbol{C}$	Damping matrix
$\boldsymbol{C}_q$	Generalized damping matrix
$\boldsymbol{F}_{\mathrm{b}}$	Buffeting forces array
$\boldsymbol{F}_{\mathrm{se}}$	Self-excited aerodynamic forces array
$\boldsymbol{H}$	Frequency response matrix
$\boldsymbol{I}$	Unit matrix
$\overline{\boldsymbol{K}}$	Net stiffness matrix
$\overline{\boldsymbol{K}}_q$	Net generalized stiffness matrix
$\boldsymbol{K}$	Stiffness matrix
$\boldsymbol{K}_q$	Generalized stiffness matrix
$\overline{\boldsymbol{M}}$	Net mass matrix
$\overline{\boldsymbol{M}}_q$	Net generalized mass matrix
$\boldsymbol{M}$	Mass matrix
$\boldsymbol{M}_q$	Generalized mass matrix
$\boldsymbol{Q}_b$	Modal generalized buffeting forces array
$\boldsymbol{Q}_{se}$	Modal generalized self-excited aerodynamic forces array
$\boldsymbol{R}_{ZZ}$	Autocovariance of $\boldsymbol{Z}$
$\boldsymbol{S}_{ZZ}$	PSD of $\boldsymbol{Z}$
$\boldsymbol{S}_{\boldsymbol{Q}_b\boldsymbol{Q}_b}$	PSD of the generalized buffeting force
$\boldsymbol{W}$	Wiener process (Standard Brownian motion)
$\boldsymbol{X}$	State vector including Gaussian buffeting forces
$\boldsymbol{Z}$	Gaussian buffeting forces approximated by the Ornstein–Uhlenbeck process
$\widetilde{\boldsymbol{Z}}$	Underlying multivariate Gaussian buffeting forces vector
$\boldsymbol{d}$	Displacement array
$\mathbf{g}_j$	Hermit polynomial coefficients array
$\boldsymbol{g}(\boldsymbol{X},t)$	Drift vector in Itô equation
$\boldsymbol{h}(\boldsymbol{X},t)$	Diffusion matrix in Itô equation
$\boldsymbol{q}$	Modal generalized coordinates
$\boldsymbol{\Phi}$	Modal shapes matrix
$\boldsymbol{\alpha}$	Time relaxing coefficients matrix
$\mathbb{K}$	Covariance matrix of $\boldsymbol{Z}$
$\boldsymbol{\Theta}$	Diffusing matrix
$\boldsymbol{\phi}_i$	Aerodynamic phase lag matrix
$\boldsymbol{\phi}_{q,i}$	Generalized aerodynamic phase lag matrix
A_i	Reference area
$A_{u,i}$, $A_{w,i}$, $B_{u,i}$, $B_{w,i}$, $B_{uw,i}$	Coefficient of the generalized buffeting force $Q_{b,i}$
B	Bridge deck width
C_D	Drag coefficient
C_D^{e}	Second derivative of the drag coefficient in terms of attack angle
C_D'	Derivative of the drag coefficient in terms of attack angle
C_L	Lift coefficient
C_L'	Derivative of the lift coefficient in terms of attack angle
C_M	Torque coefficient
C_M'	Derivative of the torque coefficient in terms of attack angle
Coh_u	Coherence function of along-wind turbulence along the span direction
Coh_w	Coherence function of vertical turbulence along the span direction
D_{b}	Aerodynamic buffeting drag forces in average wind coordinates
F_D	Aerodynamic buffeting drag forces in instantaneous wind coordinates
F_L	Aerodynamic buffeting lift forces in instantaneous wind coordinates
F_M	Aerodynamic buffeting torque in instantaneous wind coordinates
I_u, I_w	Turbulence intensity of u and w
L_u, L_w	Turbulence integral length of u and w
L_{b}	Aerodynamic buffeting lift forces in average wind coordinates
M_{b}	Aerodynamic buffeting torque in average wind coordinates
$S_{F_{b,i}F_{b,i}F_{b,i}F_{b,i}}$	High-order force spectrum
$S_{u^2u^2}$	PSD of quadratic along-wind turbulence
$S_{u^2w^2}$	Cross PSD of quadratic turbulence
S_{uu}	PSD of along-wind turbulence
$S_{w^2w^2}$	PSD of quadratic vertical turbulence
S_{ww}	PSD of vertical turbulence
T	Observation duration
U	Mean wind speed
U_{10}	Mean wind speed at 10 m height
U_e	Effective wind speed considering the motion of the bridge section
$\overline{U}_{r,i}$	Relative average wind speed
a, a_i	Power of the displacement d_i
b, b_i	Power of the velocity $\dot{d}_i$
c_u	Coefficient of the coherence function Coh_u
c_w	Coefficient of the coherence function Coh_w
$d_{se,i}$	Self-excited force phase delay
f, f_i	Power of the load Z_i
g	Gaussian peak factor
g_{ng}	Non-Gaussian peak factor
h	Vertical displacement
h_L	Tower height
$h_{\max,0}$	Extreme vertical response without the nonlinear velocity terms
$h_{\max}$	Extreme vertical response
l	Bridge length
$m(\ )$	Moments function of $\boldsymbol{X}$
n	HZ frequency
n_{dof}	DOF number
n_{se}	Number of the aerodynamic lag coefficients
p	Lateral displacement

There are two main sources of non-Gaussianity in wind loads: (1) non-Gaussian turbulence under a nature wind field (Xu et al., 2022b,a) and (2) nonlinearity from the squared components of the turbulence and geometric relations (Denoël and Degée, 2006b,a). Under the second condition, the non-Gaussian wind load is a nonlinear function of Gaussian turbulence. For these two types of non-Gaussian wind loads,

s	Order of OU polynomial process
u	Along-wind wind speed component
u_*	Friction length
$u_{r,i}$	Relative fluctuating wind speed
w	Vertical wind speed component
z	Height of main girder
$\mathbb{E}$	Expectation operator
$\mathbb{N}$	Set of all natural numbers
$\mathbb{h}_3$, $\mathbb{h}_4$, κ	Hermite polynomial coefficients of the buffeting response
α	Torsional displacement
α_0	Static wind attack angle
α_e	Effective attack angle considering the motion of the bridge section
$\alpha_{\max,0}$	Extreme torsional response without nonlinear velocity terms
$\alpha_{\max}$	Extreme torsional response
$\Delta\alpha$	Additional wind attack angle
γ	Euler constant
γ_3	Response skewness
γ_4	Response kurtosis
$\imath$	Unit virtual number
ν	Upcrossing rate
ν_{ng}	Non-Gaussian upcrossing rate
ω_0	Natural frequency of tower
ρ	Air density
σ_h	STD of the vertical response
$\sigma_{\alpha,0}$	STD of the torsional response without the nonlinear velocity terms
σ_α	STD of the torsional response
$\sigma_{h,0}$	STD of the vertical response without the nonlinear velocity terms
τ	Time delay
θ	Power of wind speed profile
ω	Circular frequency
$\xi(\ )$	Arbitrary numerical function of $\boldsymbol{X}$ at time t
ξ_0	Damping ratio of the tower

studying the transfer relationship of non-Gaussianity from excitation to response is the core of extreme value analysis. The high-order frequency domain method, whose theory naturally extends from the original frequency domain analysis, has a strict mathematical basis and depicts the high-order statistics in the frequency domain. By means of a high-order frequency spectrum (Gusella and Materazzi, 2000) or transfer function (Kareem et al., 1998), researchers calculated the non-Gaussian peak factors and discussed the evolution of non-Gaussianity with the dynamic characteristics of structures. Unfortunately, the extensive computational effort, which increases exponentially with the order of the moment spectrum and the number of DOFs, greatly reduces the applicability of this method (Gusella and Materazzi, 2000; Fan et al., 2022). Therefore, higher-order spectral analysis is more similar to a theoretical concept rather than a practical algorithm.

As another classical approach for wind-induced vibration analysis, the time domain method has been used by some scholars many years ago to calculate buffeting responses in various wind environments (Augusti et al., 1986; Deodatis, 1996; Chen and Kareem, 2001). The time domain method generates the corresponding wind load samples according to the statistical characteristics of the simulated buffeting forces. The structural responses are then calculated by structural dynamics theory, and the high-order statistical moments and spectral characteristics can be investigated from the response samples. Since the time domain analysis is theoretically suitable for arbitrary non-Gaussian excitation, some meaningful knowledge regarding non-Gaussian turbulence can be obtained. For example, Xu et al. (2022b) found that the vertical responses along the bridge deck are close to the Gaussian distribution under the influence of non-Gaussian wind, while the lateral extreme response is sensitive to the skewness of the along-wind fluctuating velocity. However, the accuracy of the time-domain analysis results largely depends on the length and time interval of the input excitations. Based on the approximation principle of the law of large numbers, the accuracy of the calculation results increases with the number of excitation samples, which will consume a large amount of computational resources.

In addition to the time domain method and the frequency domain method, the moment equation method is also a feasible algorithm. This method assumes that the non-Gaussian stochastic process obeys a specific form, such as the delta correlated non-Gaussian process (Papadimitriou, 1995), Gaussian polynomial process (Grigoriu and Ariaratnam, 1988) and polynomial filtering Gaussian white noise process (Di Paola and Falsone, 1997). Once this assumption is satisfied, the response moments can be quickly computed based on a particular set of linear equations (Denoël and Degée, 2006a). For non-Gaussian loads in the form of the polynomial of the OU process, Grigoriu (Grigoriu and Ariaratnam, 1988) used Itô's differentiation rule (Karlin and Taylor, 1981) to establish moment equations for SDOF linear systems. This method was later summarized as the state augmentation method (Grigoriu, 2002) and was successfully used to calculate the turbulence-induced vibration of a simply supported thin flat plate considering the quadratic term of turbulence. For the aerodynamic problem of long-span bridges, the aerodynamic damping and stiffness matrices in the motion governing equations are often nonclassical; thus, the coupled multiple DOFs (MDOF) system makes it difficult to apply the original state augmentation method. Cui et al. (2022) developed a MDOF state augmentation method by using multivariate OU processes and successfully evaluated the influence of non-Gaussian turbulence on the buffeting responses by this method. Derived from the theory of stochastic differential equations, the state augmentation method has developed into a favourable method for studying non-Gaussian loads with the convenience of solving linear equations.

Compared with non-Gaussian turbulence (Xu et al., 2022b; Gong and Chen, 2014; Cui et al., 2021), researchers pay less attention to the non-Gaussianity coming from nonlinear velocity terms. Because of inefficiency and computational complexity, most existing algorithms in application are limited to SDOF dynamic systems (Soize, 1978; Kareem et al., 1998) or ignore the 4th-order moments (Gusella and Materazzi, 2000), and rarely involve modal coupling long-span bridges. In this paper, the state augmentation method is utilized to discuss the influence of the second source of non-Gaussianity. Two wind-sensitive structures, a SDOF high-rise tower and a long-span bridge, are used to analyse the influence of quadratic terms on response STD, skewness, kurtosis, peak factors and extreme values.

2. Buffeting response analysis under strong turbulence

2.1. Peak responses

For slender structures with n_{dof} DOFs, the structural motion governing equation under wind loads can be described by

$$\boldsymbol{M}\ddot{\boldsymbol{d}} + \boldsymbol{C}\dot{\boldsymbol{d}} + \boldsymbol{K}\boldsymbol{d} = \boldsymbol{F}_{se} + \boldsymbol{F}_b \tag{1}$$

where $\boldsymbol{M}$, $\boldsymbol{C}$ and $\boldsymbol{K}$ are the mass, damping and stiffness matrices, respectively; $\boldsymbol{d}$ is the displacement vector; and $\boldsymbol{F}_{se}$ and $\boldsymbol{F}_b$ represent the self-excited aerodynamic force caused by the aeroelastic effect and the random aerodynamic force generated by turbulence, respectively. The self-excited force $\boldsymbol{F}_{se}$ can be expressed as $\boldsymbol{F}_{se}(\ddot{\boldsymbol{d}}, \dot{\boldsymbol{d}}, \boldsymbol{d})$, so the structure

matrices $\boldsymbol{M}$, $\boldsymbol{C}$, $\boldsymbol{K}$ will be transformed into $\overline{\boldsymbol{M}}$, $\overline{\boldsymbol{C}}$, $\overline{\boldsymbol{K}}$ by moving the self-excited force to the left side of the motion equation:

$$\overline{\boldsymbol{M}}\ddot{\boldsymbol{d}} + \overline{\boldsymbol{C}}\dot{\boldsymbol{d}} + \overline{\boldsymbol{K}}\boldsymbol{d} = \boldsymbol{F}_b \tag{2}$$

The random aerodynamic force $\boldsymbol{F}_b$ at the ith point is expressed as $\frac{1}{2}\rho(\overline{U}_{r,i}+u_{r,i})^2 C_{F_i} A_i$. $\overline{U}_{r,i}$ is the relative mean wind speed at the ith point; $u_{r,i}$ is the relative fluctuating wind speed; ρ is the air density; A_i is the reference area; and C_{F_i} is the transfer coefficient from the wind pressure to the buffeting force. Usually, $u_{r,i}^2$ is not taken into account if the turbulence intensity is at a moderate level, so the structural response strictly obeys Gaussian distribution. The peak factor can be calculated by Davenport's Gaussian model (Davenport, 1964) .

$$g = \sqrt{2\ln \nu T} + \frac{\gamma}{\sqrt{2\ln \nu T}} \tag{3}$$

where γ is the Euler constant (0.5772); ν is the cyclic rate; and T is the observation duration, which is usually 600 s. However, when the turbulence intensity is high, the turbulence quadratic term $u_{r,i}^2(t)$ amplifies extreme responses significantly by changing the response high moments (Kareem et al., 1998). For non-Gaussian random responses, Davenport's Gaussian model must be improved by employing the moment-based Hermite transformation (Gurley et al., 1997) to contain non-Gaussian characteristics.

$$\begin{aligned}
&g_{ng} = \kappa\left\{\beta + \frac{\gamma}{\beta} + \mathbb{h}_3(\beta^2+2\gamma-1) + \mathbb{h}_4\left[\beta^3 + 3\beta(\gamma-1) + \frac{3}{\beta}\left(\frac{\pi^2}{12} - \gamma + \frac{\gamma^2}{2}\right)\right]\right\}\\
&\nu_{ng} = \frac{\sigma_d}{2\pi\sigma_{\dot{d}}}(\kappa(1+4\mathbb{h}_3^2+18\mathbb{h}_4^2))^{-1}, \quad \beta = \sqrt{2\ln \nu_{ng} T}\\
&\kappa = \frac{1}{\sqrt{1+2\mathbb{h}_3^2+6\mathbb{h}_4^2}}, \mathbb{h}_3 = \frac{\gamma_3}{4+2\sqrt{1+1.5\gamma_4}}, \mathbb{h}_4 = \frac{\sqrt{1+1.5\gamma_4}-1}{18}
\end{aligned} \tag{4}$$

where σ_d and $\sigma_{\dot{d}}$ are the STDs of the displacement response and velocity response respectively; $\mathbb{h}_3$ and $\mathbb{h}_4$ are the coefficients determined by skewness and kurtosis; and γ_3 and γ_4 are the response skewness and excessive kurtosis (kurtosis minus 3), respectively.

2.2. The high-order state augmentation method

For a linear dynamic system under stationary non-Gaussian excitations, solving the 3rd-order and 4th-order response moments is very important for extreme response analysis. In this paper, a moment augmentation method based on Itô's lemma is used to compute high-order statistics (Cui et al., 2022). The non-Gaussian buffeting force $\boldsymbol{F}_b(t)$ can be approximated as the polynomial of the underlying Gaussian process $\widetilde{\boldsymbol{Z}}(t)$ (Kareem and Zhao, 1994):

$$\boldsymbol{F}_b(t) \approx \sum_{j=0}^{s} \mathbf{g}_j \widetilde{\boldsymbol{Z}}^j(t) \tag{5}$$

in which $\mathbf{g}_j$ is the polynomial coefficient and s is the order of the polynomial expansion. Some authors proposed to replace the actual Gaussian process $\widetilde{\boldsymbol{Z}}(t)$ with the OU process $\boldsymbol{Z}(t)$ (Denoël and Degée, 2006a); moreover, the OU processes are stationary Gauss–Markov processes that satisfy the following SDE:

$$\begin{aligned}
&d\boldsymbol{Z} = -\boldsymbol{\alpha}\boldsymbol{Z}dt + \boldsymbol{\Theta}d\boldsymbol{W}(t)\\
&\boldsymbol{\Theta}\boldsymbol{\Theta}^T = \boldsymbol{\alpha}\mathbb{K} + \mathbb{K}\boldsymbol{\alpha}^T
\end{aligned} \tag{6}$$

in which $\boldsymbol{\alpha}$ is the drift term of $\boldsymbol{Z}(t)$, and the eigenvalues of the matrix $-\boldsymbol{\alpha}$ have negative real parts; $\boldsymbol{\Theta}$ is the diffusion term of $\boldsymbol{Z}(t)$; $\boldsymbol{W}(t)$ is the multivariate Brownian motion, and $\boldsymbol{W}(t_2) - \boldsymbol{W}(t_1)$ obeys the Gaussian distribution with the mathematical expectation 0 and variance matrix $(t_2 - t_1)\boldsymbol{I}$ ($\boldsymbol{I}$ is the unit matrix); and $\mathbb{K}$ is the covariance matrix of $\boldsymbol{Z}(t)$. The autocorrelation function matrix and PSD matrix of the multivariate OU process $\boldsymbol{Z}(t)$ can be obtained by the following relationship:

$$\begin{aligned}
&\boldsymbol{R}_{\boldsymbol{Z}\boldsymbol{Z}}(\tau) = \exp\{-\boldsymbol{\alpha}|\tau|\mathbb{K}\}\\
&\boldsymbol{S}_{\boldsymbol{Z}\boldsymbol{Z}}(\omega) = (-\imath\omega\boldsymbol{I} + \boldsymbol{\alpha})^{-1}\left(\boldsymbol{\alpha}\mathbb{K} + \mathbb{K}\boldsymbol{\alpha}^T\right)\left(-\imath\omega\boldsymbol{I} + \boldsymbol{\alpha}^T\right)^{-1}
\end{aligned} \tag{7}$$

in which $\imath$ is an imaginary unit. Eq. (1), Eq. (5) and (6) can be reorganized as:

$$\begin{aligned}
d\begin{bmatrix}\boldsymbol{d}(t)\\ \dot{\boldsymbol{d}}(t)\\ \boldsymbol{Z}(t)\end{bmatrix} &= \begin{bmatrix}\boldsymbol{0} & \boldsymbol{I} & \boldsymbol{0}\\ -\boldsymbol{M}^{-1}\boldsymbol{K} & -\boldsymbol{M}^{-1}\boldsymbol{C} & -\boldsymbol{M}^{-1}\sum_{j=0}^{s}\mathbf{g}_j\boldsymbol{Z}^{j-1}(t)\\ \boldsymbol{0} & \boldsymbol{0} & -\boldsymbol{\alpha}\end{bmatrix}\begin{bmatrix}\boldsymbol{d}(t)\\ \dot{\boldsymbol{d}}(t)\\ \boldsymbol{Z}(t)\end{bmatrix}dt\\
&+\begin{bmatrix}\boldsymbol{0}\\ \boldsymbol{0}\\ \boldsymbol{\Theta}\end{bmatrix}d\boldsymbol{W}(t)
\end{aligned} \tag{8}$$

Eq. (8) can be written as

$$\begin{aligned}
&d\boldsymbol{X}(t) = \boldsymbol{g}(\boldsymbol{X}(t),t)dt + \boldsymbol{h}(\boldsymbol{X}(t),t)d\boldsymbol{W}(t)\\
&\boldsymbol{g}(\boldsymbol{X}(t),t) = \begin{bmatrix}\boldsymbol{0} & \dot{\boldsymbol{d}}(t) & \boldsymbol{0}\\ -\boldsymbol{M}^{-1}\boldsymbol{K}\boldsymbol{d}(t) & -\boldsymbol{M}^{-1}\boldsymbol{C}\dot{\boldsymbol{d}}(t) & -\boldsymbol{M}^{-1}\sum_{j=0}^{s}\mathbf{g}_j\boldsymbol{Z}^j(t)\\ \boldsymbol{0} & \boldsymbol{0} & -\boldsymbol{\alpha}\boldsymbol{Z}(t)\end{bmatrix}\\
&\boldsymbol{h}(\boldsymbol{X}(t),t) = \begin{bmatrix}\boldsymbol{0}\\ \boldsymbol{0}\\ \boldsymbol{\Theta}\end{bmatrix}
\end{aligned} \tag{9}$$

in which the state vector is $\boldsymbol{X}(t) = \left[\boldsymbol{d}(t), \dot{\boldsymbol{d}}(t), \boldsymbol{Z}(t)\right]^T$. ξ is defined as the power function of the state vector, $\xi = \xi(\boldsymbol{X}(t),t) = \prod_{i=1}^{n_{dof}} d_i^{a_i}(t) \prod_{i=1}^{n_{dof}} \dot{d}_i^{b_i}(t) \prod_{i=1}^{n_{dof}} Z_i^{f_i}(t)$, a_i, b_i and $f_i \in \mathbb{N}$; moreover, the expectation $\mathbb{E}[\xi]$ is noted as $\mathbb{E}[\xi] = m(a_1,\ldots,a_{n_{dof}};b_1,\ldots,b_{n_{dof}};f_1,\ldots,f_{n_{dof}})$. According to Itô's lemma, $\mathbb{E}[\xi]$ can be expressed as

$$\frac{d\mathbb{E}[\xi]}{dt} = \mathbb{E}\left[\frac{\partial\xi}{\partial t}\right] + \sum_{i=1}^{n_{dof}}\mathbb{E}\left[\frac{\partial\xi}{\partial X_i}g_i\right] + \frac{1}{2}\sum_{i,j=1}^{n_{dof}}\mathbb{E}\left[(\boldsymbol{h}\boldsymbol{h}^T)_{ij}\frac{\partial^2\xi}{\partial X_i\partial X_j}\right] \tag{10}$$

For the stationary process, $\frac{d\mathbb{E}[\xi]}{dt}$ and $\mathbb{E}\left[\frac{\partial\xi}{\partial t}\right]$ are equal to zero, and each term in Eq. (10) only shows a power change in the derivation process. $\mathbb{E}[\xi]$ will be decomposed into

$$\begin{aligned}
0 =& \sum_{j=1}^{n_{dof}} a_j\mathbb{E}\left[\prod_{i=1}^{n_{dof}} d_i^{a_i}\prod_{i=1}^{n_{dof}}\dot{d}_i^{b_i}\prod_{i=1}^{n_{dof}}Z_i^{f_i}\cdot d_j^{-1}g_j\right]\\
&+\sum_{j=n_{dof}+1}^{2n_{dof}} b_{j-n_{dof}}\mathbb{E}\left[\prod_{i=1}^{n_{dof}} d_i^{a_i}\prod_{i=1}^{n_{dof}}\dot{d}_i^{b_i}\prod_{i=1}^{n_{dof}}Z_i^{f_i}\cdot \dot{d}_{j-n_{dof}}^{-1}g_j\right]\\
&+\sum_{j=2n_{dof}+1}^{3n_{dof}} f_{j-2n_{dof}}\mathbb{E}\left[\prod_{i=1}^{n_{dof}} d_i^{a_i}\prod_{i=1}^{n_{dof}}\dot{d}_i^{b_i}\prod_{i=1}^{n_{dof}}Z_i^{f_i}\cdot Z_{j-2n_{dof}}^{-1}g_j\right]\\
&+\frac{1}{2}\sum_{j_1=2n_{dof}+1,j_2=2n_{dof}+1,j_1\neq j_2}^{3n_{dof},3n_{dof}} f_{j_1-2n_{dof}}f_{j_2-2n_{dof}}\left(\boldsymbol{h}\boldsymbol{h}^T\right)_{j_1j_2}\\
&\mathbb{E}\left[\prod_{i=1}^{n_{dof}} d_i^{a_i}\prod_{i=1}^{n_{dof}}\dot{d}_i^{b_i}\prod_{i=1}^{n_{dof}}Z_i^{f_i}\cdot Z_{j_1-2n_{dof}}^{-1}Z_{j_2-2n_{dof}}^{-1}\right]\\
&+\frac{1}{2}\sum_{j=2n_{dof}+1}^{3n_{dof}} f_{j-2n_{dof}}(f_{j-2n_{dof}}-1)\left(\boldsymbol{h}\boldsymbol{h}^T\right)_{jj}\\
&\mathbb{E}\left[\prod_{i=1}^{n_{dof}} d_i^{a_i}\prod_{i=1}^{n_{dof}}\dot{d}_i^{b_i}\prod_{i=1}^{n_{dof}}Z_i^{f_i}\cdot Z_{j-2n_{dof}}^{-2}\right]
\end{aligned} \tag{11}$$

The Eq. (11) is a linear equation composed of excitation moments and response moments. The $m(0,\ldots,a_r,\ldots,0;0,\ldots,0;0,\ldots,0)$, which is the a_r-th moment of the displacement $d_r(t)$, can be obtained from Eq. (11) through subsequently increasing $\sum_{i=1}^{n_{dof}}(a_i+b_i)$ from 1 to s. Generally, the order of the OU polynomial process s is 3, so a total of 22 linear equations should be established to obtain the 4th-order moments. More specifically, the calculations of the moments $m(a_1,\ldots,a_{n_{dof}};b_1,\ldots,b_{n_{dof}};f_1,\ldots,f_{n_{dof}})$ for $\sum_{i=1}^{n_{dof}}(a_i+b_i)=1$, $\sum_{i=1}^{n_{dof}} f_i = 0,1,\ldots,9$; $\sum_{i=1}^{n_{dof}}(a_i+b_i)=2$, $\sum_{i=1}^{n_{dof}} f_i = 0,1,\ldots,6$;

$\sum_{i=1}^{n_{dof}}(a_i+b_i)=3$, $\sum_{i=1}^{n_{dof}} f_i=0,1,2,3$ until $\sum_{i=1}^{n_{dof}}(a_i+b_i)=4$, $\sum_{i=1}^{n_{dof}} f_i=0$ are required.

2.3. Comparison of the frequency method and state augmentation method

The computational efficiency of the frequency domain method and the state augmentation method will be discussed in this section. In the frequency domain approach, the frequency response functions defined in complex domains are often used to generate response spectra from force spectra. This calculation mode can be summarized as "spectrum to spectrum". To consider the non-Gaussian characteristics caused by quadratic terms, the response spectra must be extended to the bi-spectrum and tri-spectrum to contain more statistical moment information (Gusella and Materazzi, 2000). The response spectra from 2nd to 4th could be represented as

$$\begin{aligned}
S_{d_{i_1}d_{i_2}}(\omega_1) &= \sum_{j_1=1}^{n_{dof}}\sum_{j_2=1}^{n_{dof}} H^*_{i_1j_1}(\omega_1)H_{i_2j_2}(\omega_1)S_{F_{b,j_1}F_{b,j_2}}(\omega_1)\\
S_{d_{i_1}d_{i_2}d_{i_3}}(\omega_1,\omega_2) &= \sum_{j_1=1}^{n_{dof}}\sum_{j_2=1}^{n_{dof}}\sum_{j_3=1}^{n_{dof}} H^*_{i_1j_1}(\omega_1+\omega_2)H_{i_2j_2}(\omega_1)H_{i_3j_3}(\omega_2)\\
&\quad\times S_{F_{b,j_1}F_{b,j_2}F_{b,j_3}}(\omega_1,\omega_2)\\
S_{d_{i_1}d_{i_2}d_{i_3}d_{i_4}}(\omega_1,\omega_2,\omega_3) &= \sum_{j_1=1}^{n_{dof}}\sum_{j_2=1}^{n_{dof}}\sum_{j_3=1}^{n_{dof}}\sum_{j_4=1}^{n_{dof}}\\
&\quad\times H^*_{i_1j_1}(\omega_1+\omega_2+\omega_3)H_{i_2j_2}(\omega_1)H_{i_3j_3}(\omega_2)H_{i_3j_3}(\omega_3)\\
&\quad\times S_{F_{b,j_1}F_{b,j_2}F_{b,j_3}F_{b,j_4}}(\omega_1,\omega_2,\omega_3)
\end{aligned} \tag{12}$$

Here, $H_{i_1j_1}$ represents the frequency response function, and $H^*_{i_1j_1}$ is the conjugate of $H_{i_1j_1}$. With the increase in the order of moment spectra, not only does the amount of multiple summation increase, but the dimension of frequency domain decomposition also becomes larger. The incredible calculation amount makes it unrealistic to consider non-Gaussian information of external loads, especially kurtosis, in MDOF structures. Therefore, Eq. (12) can be seen as a theoretical formula rather than an available analytical tool. In the state augmentation method, the "spectrum to spectrum" mode is replaced by "moment to moment" to avoid a large number of multiple integral and product operations. As long as the wind load belongs to the load type given in advance, 22 moment equations can be established to solve the response moments very quickly, which greatly improves the computational efficiency (Denoël and Degée, 2006a).

3. Buffeting responses of a SDOF tower

3.1. Aerodynamic loading modal and analysis

The first example is a SDOF tower (see Fig. 1), which is a classic engineering case used by many scholars to study the influence of quadratic terms (Kareem et al., 1998; Soize, 1978; Grigoriu, 1984). The structure motion equation in the along-wind direction can be expressed as follows:

$$m_1\ddot{d}+c_1\dot{d}+k_1 d=\frac{1}{2}\rho A_1 C_D(U+u-\dot{d})^2 \tag{13}$$

where C_D is the along-wind force coefficient; U is the mean wind velocity; and u is the fluctuating wind speed. If the effect of aerodynamic damping is not considered, the motion velocity terms $(U+u)\dot{d}$ and $\dot{d}^2$ can be ignored, and the motion control equation can be expressed as

$$\ddot{d}+\frac{c_1}{m_1}\dot{d}+\frac{k_1}{m_1}d=\frac{\rho A C_D U^2}{m_1}\frac{u}{U}+\frac{\rho A C_D U^2}{2m_1}\frac{u^2}{U^2} \tag{14}$$

It is assumed that the dimensionless buffeting force $Z_1(t)=u(t)/U$ can be represented as the OU process satisfying the stochastic differential equation:

$$dZ_1(t)=-\alpha_1 Z_1(t)dt+\frac{\sigma_u\sqrt{2\alpha_1}}{U}dW_1(t) \tag{15}$$

, and the PSD of $Z_1(t)$ is given by

$$S_{Z_1Z_1}(n)=\frac{4\sigma_u^2\alpha_1}{U^2(4\pi^2n^2+\alpha_1^2)} \tag{16}$$

in which α_1 is the drift term of the 1-D OU process, n is the HZ frequency, and σ_u is the STD of fluctuating wind. The governing equation can be represented as

$$\begin{aligned}
d\begin{bmatrix} d\\ \dot{d}\\ Z_1\end{bmatrix} &= \begin{bmatrix} 0 & 1 & 0\\ -\frac{k_1}{m_1} & \frac{c_1}{m_1} & \frac{\rho A C_D U^2}{m_1}+\frac{\rho A C_D U^2}{2m_1}Z_1\\ 0 & 0 & -\alpha_1\end{bmatrix}\begin{bmatrix} d\\ \dot{d}\\ Z_1\end{bmatrix}dt\\
&\quad+\begin{bmatrix} 0\\ 0\\ \frac{\sigma_u\sqrt{2\alpha_1}}{U}\end{bmatrix}dW_1(t)
\end{aligned} \tag{17}$$

Applying Eq. (11), the moment equation of state vector $\boldsymbol{X}(t)=[d(t),\dot{d}(t),Z_1(t)]^T$ is

$$\begin{aligned}
0 &= am(a-1,b+1,f)-bk_1m(a+1,b-1,f)\\
&\quad-(bc_1+f\alpha)m(a,b,f)+\frac{a\rho AC_DU^2}{m_1}m(a,b-1,f+1)\\
&\quad+\frac{b\rho AC_DU^2}{2m_1}m(a,b-1,f+2)+f(f-1)\alpha_1\frac{\sigma_u^2}{U^2}m(a,b,f-2)
\end{aligned} \tag{18}$$

$$m(a,b,f)=\mathbb{E}\left[d^a(t)\dot{d}^b(t)Z_1^f(t)\right] \tag{19}$$

The 4th-order moment of response $m(4,0,0)$ must be determined by solving the equations when $a+b=4$, $f=0$; $a+b=3$, $f=0\sim2$; $a+b=2$, $f=0\sim4$; $a+b=1$, $f=0\sim6$. Since the maximum power of the OU process in Eq. (14) is 2, a total of 16 linear equations are solved instead of 22 linear equations.

3.2. The calculation of the peak factors

The response peak factors obtained by different methods are illustrated in Table 1. The drift term α_1 is obtained by fitting the buffeting force spectrum with the OU process at natural frequency in Fig. 2. The wind spectrum given in Grigoriu (1984) is chosen to calculate the buffeting force spectrum $S_{Z_1Z_1}$. Because the error between the spectra is sufficiently small, the results show that the state augmentation method and Kareem's calculation results are close in all cases and prove that the introduction of the OU process to replace the buffeting force does not cause much error.

4. Buffeting responses of large-span bridges

4.1. The buffeting force with quadratic terms

Compared with the SDOF structure, the buffeting response of long-span bridges under natural wind turbulence is more important. As shown in Fig. 3, the main girder is affected by the fluctuating winds u and w at the same time. The average wind attack angle under the structural equilibrium state at a certain time is α_0, and the additional wind attack angle caused by fluctuating winds is defined as $\Delta\alpha$. Based on the specified positive direction in Fig. 3, the relative attack angle α_e and wind velocity U_e can be expressed by

$$\begin{aligned}
\alpha_e(t) &= \arctan\left(\frac{w(t)+\dot{h}(t)}{U+u(t)-\dot{p}(t)}\right)+\alpha_0+\alpha(t)\\
U_e^2(t) &= (U+u(t)-\dot{p}(t))^2+(w(t)+\dot{h}(t))^2
\end{aligned} \tag{20}$$

In Davenport's buffeting force model, the stochastic lifting force independent of displacement under a fluctuating wind load can be expressed as

$$F_L(t)=\frac{1}{2}\rho\left[1+2\frac{u(t)}{U}+\left(\frac{u(t)}{U}^2\right)+\left(\frac{w(t)}{U}^2\right)\right]BC_L(\alpha_0+\Delta\alpha) \tag{21}$$

Table 1
Comparison of peak factors.

Case	U_{10} (m/s)	θ	U (m/s)	σ_u (m/s)	ξ_0 (%)	g Kareem et al. (1998)	g Present	g_{ng} Kareem et al. (1998)	g_{ng} Present
h_L = 20 m; m_1 = 2161 kg; $\omega_0 = 2\ \pi$									
1	28	0.15	31.00	4.6	5	4.04	4.01	5.09	5.09
2	13	0.35	16.57	5.8	3	4.10	4.06	6.50	6.34
3	13	0.35	16.57	5.8	5	4.04	4.01	6.44	6.40
h_L = 80 m; m_1 = 13500 kg; $\omega_0 = 0.8\ \pi$									
4	28	0.15	38.25	4.6	3	3.87	3.89	4.49	4.48
5	28	0.15	38.25	4.6	5	3.85	3.88	4.56	4.55
6	13	0.35	26.92	5.8	3	3.87	3.89	5.01	4.94
7	13	0.35	26.92	5.8	5	3.85	3.85	5.14	5.07

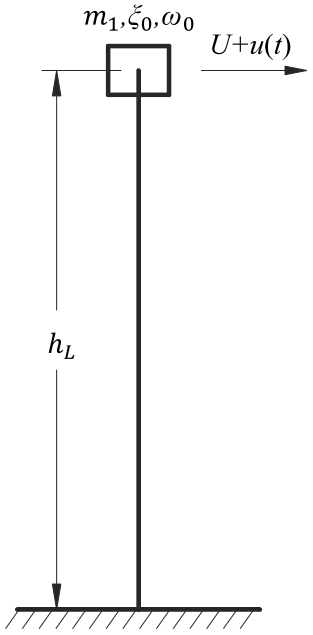

Fig. 1. Sketch of the SDOF tower.

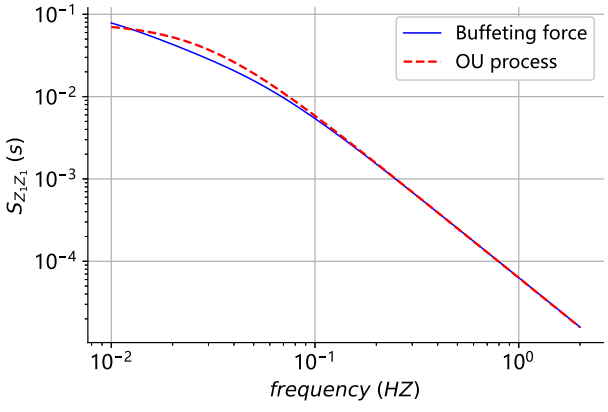

Fig. 2. Comparison of the PSD between the buffeting force and the OU process (Case 4).

and the lifting force coefficient can be expanded by the Taylor series

$$C_L(\alpha_0+\Delta\alpha) = C_L(\alpha_0) + \Delta\alpha C_L'(\alpha_0) + \frac{\Delta\alpha^2}{2}C_L''(\alpha_0) \tag{22}$$

where C_L' and C_L'' are the first derivative and the second derivative of C_L, respectively. C_L'' is ignored for simplicity, although this term is meaningful in the quadratic terms analysis.

The drag force $F_D(t)$ and pitching moment $F_M(t)$ can be obtained in the same way. The buffeting force is transformed from instantaneous wind coordinates to average wind coordinates according to geometric relations.

$$\begin{aligned} D_b(t) &= F_D(t)\cos\Delta\alpha - F_L(t)\sin\Delta\alpha \\ L_b(t) &= F_L(t)\cos\Delta\alpha + F_D(t)\sin\Delta\alpha \\ M_b(t) &= F_M(t) \\ \cos\Delta\alpha &\approx 1 - \frac{\Delta\alpha^2}{2} \\ \sin\Delta\alpha &\approx \Delta\alpha \approx \frac{w(t)}{U} \end{aligned} \tag{23}$$

Finally, the buffeting forces consisting of velocity quadratic terms are given in Eq. . Since the wind load along the bridge width direction is not completely correlated, aerodynamic admittance functions are often introduced to modify the buffeting force model. However, for the quadratic terms, there is no applicable correcting function similar to aerodynamic admittance. Thus, the aerodynamic admittance is temporarily ignored in this paper.

$$\begin{aligned} D_b(t) = \frac{1}{2}\rho U^2 B \Bigg\{ & \left[2C_D\frac{u(t)}{U} + (C_D' - C_L)\frac{w(t)}{U}\right] \\ & + \left[C_D\left(\frac{u(t)}{U}\right)^2 + \left(\frac{C_D}{2} - C_L'\right)\left(\frac{u(t)}{U}\right)^2\right] \\ & + \left[(2C_D' - 2C_L)\frac{u(t)}{U}\frac{w(t)}{U}\right]\Bigg\} \\ L_b(t) = \frac{1}{2}\rho U^2 B \Bigg\{ & \left[2C_L\frac{u(t)}{U} + (C_L' + C_D)\frac{w(t)}{U}\right] \\ & + \left[C_L\left(\frac{u(t)}{U}\right)^2 + \left(C_D' + \frac{C_L}{2}\right)\left(\frac{u(t)}{U}\right)^2\right] \\ & + \left[(2C_L' + 2C_D)\frac{u(t)}{U}\frac{w(t)}{U}\right]\Bigg\} \\ M_b(t) = \frac{1}{2}\rho U^2 B^2 \Bigg\{ & \left[2C_M\frac{u(t)}{U} + C_M'\frac{w(t)}{U}\right] \\ & + \left[C_M\left(\frac{u(t)}{U}\right)^2 + C_M\left(\frac{w(t)}{U}\right)^2\right] \\ & + \left[2C_M'\frac{u(t)}{U}\frac{w(t)}{U}\right]\Bigg\} \end{aligned}$$

4.2. The 2-dimensional state augmentation method

For the bridge section, the self-excited force $\boldsymbol{F}_{se}$ in Eq. (1) is usually described by the famous Scanlan flutter derivative theory in the frequency domain (Scanlan, 1978). Chen et al. (2000) provides a method to express the self-excited forces per unit span induced by arbitrary structural motion in the time domain, which is called the rational function approximation method known as Roger's approximation. The

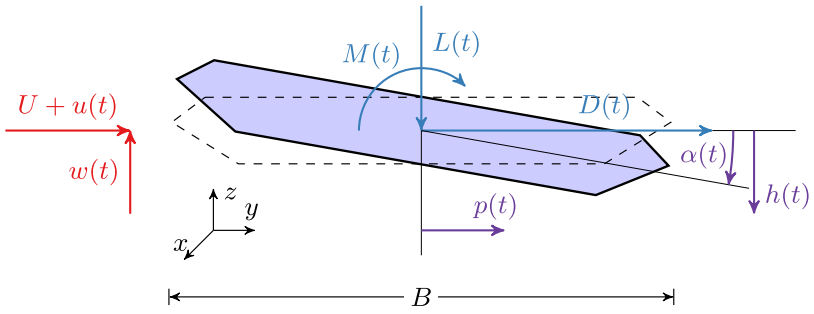

Fig. 3. Two coordinates system about aerodynamic force and bridge motion.

self-excited force vector can be written as

$$\begin{aligned} \boldsymbol{F}_{se} &= \boldsymbol{A}_1\boldsymbol{d} + \boldsymbol{A}_2\frac{B}{U}\dot{\boldsymbol{d}} + \boldsymbol{A}_3\frac{B^2}{U^2}\ddot{\boldsymbol{d}} + \sum_{i=1}^{n_{se}}\boldsymbol{\phi}_i(t) \\ \dot{\boldsymbol{\phi}}_i(t) &= -\frac{d_{se,i}U}{B}\boldsymbol{\phi}_i(t) + \boldsymbol{A}_{i+3}\dot{\boldsymbol{d}} \end{aligned} \tag{24}$$

where $\boldsymbol{A}_1$, $\boldsymbol{A}_2$, $\boldsymbol{A}_3$, $\boldsymbol{A}_{i+3}$ and $d_{se,i}$ are frequency-independent coefficients; and $\boldsymbol{\phi}_i(t)$ are new variables that are introduced to express the aerodynamic phase lag. All these coefficients can be calculated by the least-square method.

The mode coordinate $\boldsymbol{q}$ is then introduced to separate the structural mode and decouple the mass, stiffness and damping matrix of the structure, $\boldsymbol{d} = \boldsymbol{\Phi q}$.

$$\begin{aligned} &\boldsymbol{M}_q\ddot{\boldsymbol{q}} + \boldsymbol{C}_q\dot{\boldsymbol{q}} + \boldsymbol{K}_q\boldsymbol{q} = \boldsymbol{Q}_{se} + \boldsymbol{Q}_b \\ &\overline{\boldsymbol{M}}_q\ddot{\boldsymbol{q}} + \overline{\boldsymbol{C}}_q\dot{\boldsymbol{q}} + \overline{\boldsymbol{K}}_q\boldsymbol{q} = \sum_{i=1}^{n_{se}}\boldsymbol{\phi}_{q,i} + \boldsymbol{Q}_b \end{aligned} \qquad \begin{aligned} \overline{\boldsymbol{M}}_q &= \boldsymbol{M}_q - \frac{1}{2}\rho B^2\boldsymbol{A}_{q,1} \\ \overline{\boldsymbol{C}}_q &= \boldsymbol{C}_q - \frac{1}{2}\rho BU\boldsymbol{A}_{q,2} \\ \overline{\boldsymbol{K}}_q &= \boldsymbol{K}_q - \frac{1}{2}\rho U^2\boldsymbol{A}_{q,3} \end{aligned} \tag{25}$$

where $\boldsymbol{M}_q = \boldsymbol{\Phi}^T\boldsymbol{M}\boldsymbol{\Phi}$, $\boldsymbol{C}_q = \boldsymbol{\Phi}^T\boldsymbol{C}\boldsymbol{\Phi}$ and $\boldsymbol{K}_q = \boldsymbol{\Phi}^T\boldsymbol{K}\boldsymbol{\Phi}$ are the generalized mass, damping and stiffness matrices, respectively; $\boldsymbol{Q}_{se} = \boldsymbol{\Phi}^T\boldsymbol{F}_{se}$ and $\boldsymbol{Q}_b = \boldsymbol{\Phi}^T\boldsymbol{F}_b$ are the generalized self-excited force and generalized buffeting force, respectively; $\boldsymbol{\Phi}$ is the modal matrix; and $\boldsymbol{A}_{q,i} = \boldsymbol{\Phi}^T\boldsymbol{A}_i\boldsymbol{\Phi}$ $(i = 1 \sim n_{se} + 3)$ and $\boldsymbol{\phi}_{q,i} = \boldsymbol{\Phi}^T\boldsymbol{\phi}_i$ $(i = 1 \sim n_{se})$ are the parameters of generalized self-excited forces. The relationship between the ith generalized buffeting forces and wind velocities is as follows

$$\begin{aligned} Q_{b,i}(t) = \frac{1}{2}\rho U^2B^2\Bigg[&\int_0^l A_{u,i}\frac{u(x,t)}{U} + A_{w,i}\frac{w(x,t)}{U}dx \\ &+ \int_0^l B_{u,i}\frac{u^2(x,t)}{U^2} + B_{w,i}\frac{w^2(x,t)}{U^2}dx \\ &+ \int_0^l B_{uw,i}\frac{u(x,t)w(x,t)}{U^2}dx\Bigg] \end{aligned} \tag{26a}$$

$$\begin{aligned} A_{u,i} &= 2C_Lh_i(x) + 2C_Dp_i(x) + 2C_M\alpha_i(x) \\ A_{w,i} &= (C_L' + C_D)h_i(x) + (C_D' - C_L)p_i(x) + C_M'\alpha_i(x) \\ B_{u,i} &= C_Lh_i(x) + C_Dp_i(x) + C_M\alpha_i(x) \\ B_{w,i} &= (C_D' + C_L/2)h_i(x) + (C_D/2 - C_L')p_i(x) + C_M\alpha_i(x) \\ B_{uw,i} &= (2C_L' + 2C_D)h_i(x) + (2C_D' - 2C_L)p_i(x) + 2C_M'\alpha_i(x) \end{aligned} \tag{26b}$$

where l is the main span length; and $h_i(x)$, $p_i(x)$ and $\alpha_i(x)$ are the vertical, lateral and torsional displacements, respectively, under the ith mode. $A_{u,i}$, $A_{w,i}$, $B_{u,i}$, $B_{w,i}$ and $B_{uw,i}$ are the parameters related to the mode shape and the three-component force coefficients. For simplicity and without loss of generality, only the first vertical and torsional modes are considered, and aerodynamic phase lags are ignored. The 2-D case of Eqs. (8) and (11) can be expressed as

$$\begin{aligned} d\begin{bmatrix} q_1 \\ q_2 \\ \dot{q}_1 \\ \dot{q}_2 \\ Z_1 \\ Z_2 \end{bmatrix} &= \begin{bmatrix} 0 & 0 & 1 & 0 & 0 & 0 \\ 0 & 0 & 0 & 1 & 0 & 0 \\ -k_{11} & -k_{12} & -c_{11} & -c_{12} & \sum_{i=0}^{s}g_{1j}Z_1^{j-1} & 0 \\ -k_{21} & -k_{22} & -c_{21} & -c_{22} & 0 & \sum_{i=0}^{s}g_{2j}Z_2^{j-1} \\ 0 & 0 & 0 & 0 & -\alpha_{11} & -\alpha_{12} \\ 0 & 0 & 0 & 0 & -\alpha_{21} & -\alpha_{22} \end{bmatrix}\begin{bmatrix} q_1 \\ q_2 \\ \dot{q}_1 \\ \dot{q}_2 \\ Z_1 \\ Z_2 \end{bmatrix}dt \\ &+ \begin{bmatrix} 0 & 0 \\ 0 & 0 \\ 0 & 0 \\ 0 & 0 \\ \Theta_{11} & \Theta_{12} \\ \Theta_{21} & \Theta_{22} \end{bmatrix}\begin{bmatrix} dW_1(t) \\ dW_2(t) \end{bmatrix} \end{aligned} \tag{27}$$

$$\begin{aligned} 0 = &-(b_1c_{11} + b_2c_{22} + f_1\alpha_{11} + f_2\alpha_{22})m(a_1,a_2,b_1,b_2,f_1,f_2) \\ &+ a_1m(a_1-1,a_2,b_1+1,b_2,f_1,f_2) \\ &+ a_2m(a_1,a_2-1,b_1,b_2+1,f_1,f_2) \\ &- b_1k_{11}m(a_1+1,a_2,b_1-1,b_2,f_1,f_2) \\ &- b_1k_{12}m(a_1,a_2+1,b_1-1,b_2,f_1,f_2) \\ &- b_2k_{21}m(a_1+1,a_2,b_1,b_2-1,f_1,f_2) \\ &- b_2k_{22}m(a_1,a_2+1,b_1,b_2-1,f_1,f_2) \\ &- b_1c_{12}m(a_1,a_2,b_1-1,b_2+1,f_1,f_2) \\ &- b_2c_{21}m(a_1,a_2,b_1+1,b_2-1,f_1,f_2) \\ &+ b_1\sum_{j=0}^{s}g_{1j}m(a_1,a_2,b_1-1,b_2,f_1+j,f_2) \\ &+ b_2\sum_{j=0}^{s}g_{2j}m(a_1,a_2,b_1,b_2-1,f_1,f_2+j) \\ &- f_1\alpha_{12}m(a_1,a_2,b_1,b_2,f_1-1,f_2+1) \\ &- f_2\alpha_{21}m(a_1,a_2,b_1,b_2,f_1+1,f_2-1) \\ &+ f_1f_2(\Theta_{11}\Theta_{21} + \Theta_{12}\Theta_{22})m(a_1,a_2,b_1,b_2,f_1-1,f_2-1) \\ &+ \frac{1}{2}f_1(f_1-1)(\Theta_{11}^2 + \Theta_{12}^2)m(a_1,a_2,b_1,b_2,f_1-2,f_2) \\ &+ \frac{1}{2}f_2(f_2-1)(\Theta_{21}^2 + \Theta_{22}^2)m(a_1,a_2,b_1,b_2,f_1,f_2-2) \end{aligned} \tag{28}$$

$$m(a_1,a_2,b_1,b_2,f_1,f_2) = \mathbb{E}\left[q_1^{a_1}q_2^{a_2}\dot{q}_1^{b_1}\dot{q}_2^{b_2}Z_1^{f_1}Z_2^{f_2}\right] \tag{29}$$

Similar to the moment equations in SDOF structures, the 4th-order moment $m(4,0,0,0,0,0)$ and $m(0,4,0,0,0,0)$ are obtained when $a_1+a_2+b_1+b_2 = 4$, $f_1+f_2 = 0$; $a_1+a_2+b_1+b_2 = 3$, $f_1+f_2 = 0 \sim 3$; $a_1+a_2+b_1+b_2 = 2$, $f_1+f_2 = 0 \sim 6$; $a_1+a_2+b_1+b_2 = 1$, $f_1+f_2 = 0 \sim 9$.

4.3. Determination of the polynomial coefficient matrix

Assuming independence between the turbulent stochastic fields $u(x,t)$ and $w(x,t)$ (Denoël and Degée, 2006b; Gusella and Materazzi, 2000) and ignoring the imaginary part of the wind spectrum, the cross-spectral $S_{Q_{b,i}Q_{b,j}}(\omega)$ of the non-Gaussian force $Q_{b,i}$ and $Q_{b,j}$ can be expressed as follows:

$$S_{Q_{b,i}Q_{b,j}}(\omega) = \left(\frac{1}{2}\rho B^2 U^2\right)^2 \int_0^l \int_0^l A_{u,i}A_{u,j}\frac{S_{uu}}{U^2} + A_{w,i}A_{w,j}\frac{S_{ww}}{U^2} + B_{u,i}B_{u,j}\frac{S_{u^2u^2}}{U^4} + B_{w,i}B_{w,j}\frac{S_{w^2w^2}}{U^4} + B_{uw,i}B_{uw,j}\frac{S_{u^2w^2}}{U^4} dx_1 dx_2 \tag{30}$$

where S_{uu}, S_{ww}, $S_{u^2u^2}$, $S_{w^2w^2}$ and $S_{u^2w^2}$ are the cross PSDs of the corresponding subscripts. For example, S_{uu} is the cross PSD of $u(x_1,t)$ and $u(x_2,t)$, $S_{u^2u^2}$ is the cross PSD of $u^2(x_1,t)-\sigma_u^2$ and $u^2(x_2,t)-\sigma_u^2$, and $S_{u^2w^2}$ is the cross PSD of $u(x_1,t)w(x_1,t)$ and $u(x_2,t)w(x_2,t)$. According to the convolution theorem, the PSD of the quadratic terms satisfies

$$\begin{aligned} S_{u^2u^2}(x_1,x_2,\omega) &= \frac{1}{\pi}\int_{-\infty}^{+\infty} S_{uu}(x_1,x_2,\omega')S_{uu}(x_1,x_2,\omega-\omega')d\omega' \\ S_{w^2w^2}(x_1,x_2,\omega) &= \frac{1}{\pi}\int_{-\infty}^{+\infty} S_{ww}(x_1,x_2,\omega')S_{ww}(x_1,x_2,\omega-\omega')d\omega' \\ S_{u^2w^2}(x_1,x_2,\omega) &= \frac{1}{2\pi}\int_{-\infty}^{+\infty} S_{uu}(x_1,x_2,\omega')S_{ww}(x_1,x_2,\omega-\omega')d\omega' \end{aligned} \tag{31}$$

The coherence function is introduced to describe the correlation degree of two-point fluctuating wind velocities in the frequency domain, and a simple expression related only to the distance between two points but not to the frequency is adopted here.

$$\begin{aligned} S_{uu}(x_1,x_2,\omega) &= Coh_u(x_1,x_2)S_{uu}(x_1,x_1,\omega) \\ &= \exp\left(-\frac{c_u\omega|x_1-x_2|}{2\pi U}\right)S_{uu}(x_1,x_1,\omega) \\ S_{ww}(x_1,x_2,\omega) &= Coh_w(x_1,x_2)S_{ww}(x_1,x_1,\omega) \\ &= \exp\left(-\frac{c_w\omega|x_1-x_2|}{2\pi U}\right)S_{ww}(x_1,x_1,\omega) \end{aligned} \tag{32}$$

The third order Hermite polynomial is a suitable translation function that transforms the non-Gaussian process $Q_{b,i}(t)$ to the underlying standard Gaussian process $Z_i(t)$ (Winerstein, 1988):

$$\begin{aligned} Q_{b,i}(t) &= \mathbb{H}\left[Z_i(t)\right] = \sum_{j=0}^{3} \mathrm{g}_{ij} Z_i^j(t) \\ &= \kappa_i\left[Z_i(t) + \mathbb{h}_{3,i}\left(Z_i^2(t)-1\right) + \mathbb{h}_{4,i}\left(Z_i^3(t)-3Z_i(t)\right)\right] \end{aligned} \tag{33}$$

Polynomial coefficients have been defined in Eq. (4). The cross spectrum $S_{Z_iZ_j}$ of Gaussian processes Z_i and Z_j is calculated by using the spectrum distortion method on $S_{Q_{b,i}Q_{b,j}}$, which offers a closed form correlation distortion between the non-Gaussian and underlying Gaussian process (Yang and Gurley, 2015). This methodology is applicable to a wide range of mildly and strongly non-Gaussian processes.

5. Calculation results of a selected bridge

5.1. Overview and basic hypothesis of the calculated suspension bridge

A suspension bridge shown in Fig. 4 is selected for analysis. The main span of the bridge is 1263 m. The frequencies of the first vertical and torsional modes are 0.0870 Hz and 0.1916 Hz, respectively. Other parameters of the suspension bridge can be obtained from a previous paper (Cui et al., 2022) .

In the calculation of the buffeting responses, some regulations and assumptions are adopted, and they are summarized as follows:

(1) Ignoring material nonlinearity and geometric nonlinearity, the structural mass, damping and stiffness matrix are not affected by deformation and loads.

(2) Only the first vertical mode and the first torsional mode are considered in the analysis, and the above two mode shapes are sinusoidal symmetric. The order of the moment equations is sensitive to the DOF, and there are difficulties in program implementation for modes greater than 2. The lateral response p for the bridge section, which is less important in the streamlined sectional shape, is not taken into consideration for this reason.

(3) The eight flutter derivatives used by the rational function approximation method are obtained by the Theodorsen function (Theodorsen, 1935), and the aerodynamic memory effects are ignored, namely $A_{i+3}=0$ $(i=1\sim n_{se})$.

(4) The turbulence intensity I_w equals to $0.5I_u$. The von Kármán wind spectrum and Panofsky wind spectrum are selected for along-wind and vertical fluctuating wind velocities respectively; the von Kármán wind spectrum is given in Eq. (34), and Panofsky spectrum is represented in Eq. (35)

$$\frac{nS_{uu}}{\sigma_u^2} = \frac{\frac{4L_u n}{U}}{\left[1+70.8\left(\frac{L_u n}{U}\right)^2\right]^{5/6}} \tag{34}$$

$$\frac{nS_{ww}}{u_*^2} = \frac{3.36\frac{nz}{U}}{1+10\left(\frac{nz}{U}\right)^{5/3}} \tag{35}$$

(5) The Gaussian random fields $u(x,t)$ and $w(x,t)$ are assumed to be independent of each other (Denoël and Degée, 2006b; Gusella and Materazzi, 2000), and the influence of the cross-spectra of $u(x,t)$ and $w(x,t)$ are ignored. This assumption is the premise for obtaining Eq. (30).

5.2. The comparison of the response STD with the frequency domain method

Fig. 5 compares the PSD of the buffeting force and OU process when the average wind speed is $U=40\ m/s$ and the turbulence intensity is $I_u=0.21$. Generally, it is acceptable to use the OU process to depict the buffeting force in the frequency domain; however, the OU spectrum slightly deviates from the force spectrum at high frequencies. To demonstrate the effectiveness of the state augmentation method in calculating the 2nd-order moment, the response STD is also calculated by the traditional frequency domain method. Fig. 6 plots the response STD obtained by different methods, and demonstrates that the results of the proposed methods match those of the traditional frequency domain method. At some wind speeds, the relatively large deviation (approximately 15%) comes from the PSD error in Fig. 5. Theoretically, when the buffeting force obeys the OU process exactly, the results of these two methods will be completely consistent.

In addition, due to the aerodynamic coupling effect, the system stiffness and damping matrices vary asymmetrically with the wind speed. The increasing trend of the vertical response slows down due to increased vertical aerodynamic damping. Conversely, the increasing trend of the torsional response becomes higher with decreased torsional aerodynamic damping. When the wind speed approaches the critical flutter speed of 60 m/s, both the vertical and torsional responses increase rapidly.

5.3. Response STD

Figs. 7(a) and 7(b) show the STDs of the vertical and torsional responses that change with the mean wind speed U and turbulence I_u, respectively. The step gaps of the wind speed U and the turbulence intensity I_u are 5 m/s and 0.05, respectively. Obviously, both the wind speed and turbulence are dominating factors on the response STD.

In Figs. 8(a) and 8(b), the STD amplification coefficients $\sigma_h/\sigma_{h,0}$ and $\sigma_\alpha/\sigma_{\alpha,0}$ are defined to express the amplification by quadratic terms.

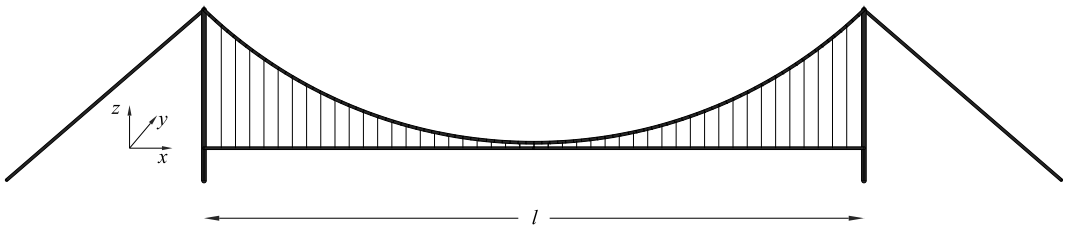

Fig. 4. Sketch of a long-span suspension bridge.

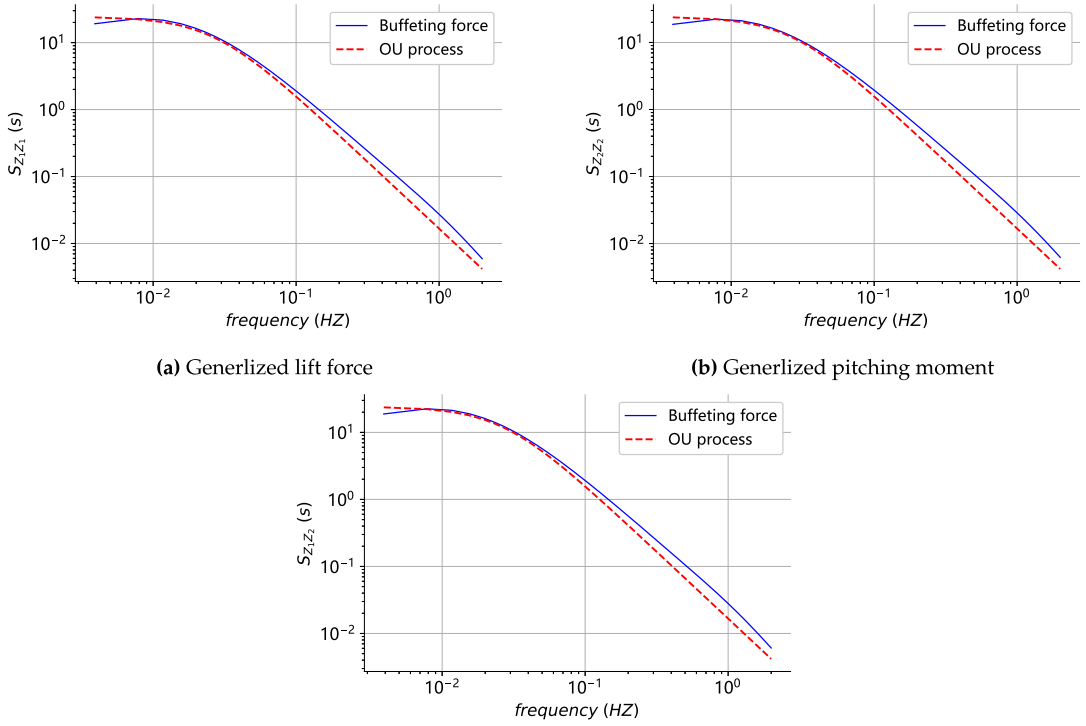

(a) Generlized lift force

(b) Generlized pitching moment

(c) Cross PSD between the lift force and moment

Fig. 5. PSD Comparison between the OU process and the Gaussian underlying buffeting forces.

$\sigma_{h,0}$ and $\sigma_{\alpha,0}$ represent the STDs of the vertical and torsional responses, respectively, without considering the nonlinear terms. Overall, the influence of the turbulence intensity on STD is more significant than that of mean speed. In Eq. (26), under high turbulence, the additional STD caused by the nonlinear terms occupies a larger proportion in the STD of the overall buffeting force, which becomes the main reason for the amplification of the response STD.

When the turbulence intensity is fixed, the spatial correlation of the turbulent flow field arises with the wind speed, so the quadratic terms have a more significantly effect on buffeting forces at high speeds. In addition, in MDOF structures, the aerodynamic damping and stiffness influence the transmission from the excitation to the response in a more complicated manner, and it is difficult to obtain the simple rule such as SDOF systems. A discussion of the SDOF system is presented in Appendix.

5.4. Response skewness and kurtosis

For non-Gaussian excitations, it is necessary to analyse the influence of turbulence quadratic terms on the response skewness and kurtosis. As shown in Figs. 9 and 10, the non-Gaussianity of responses increases monotonically with the turbulence intensity. Due to higher spatial correlation, the response non-Gaussianity will become greater at high wind speed. However, since the transmission of non-Gaussianity is significantly controlled by the system damping (Kotulski and Sobczyk, 1981), when approaching the flutter critical wind speed, the response skewness and kurtosis decrease instead because the aerodynamic damping significantly reduces the system damping. Compared with the torsional mode, the skewness and kurtosis of the vertical response begin to decrease at higher wind speeds. This phenomenon originates from the fact that vertical aerodynamic damping increases with wind speed while the torsional aerodynamic damping decreases with wind speed.

5.5. Response extreme value

The extreme responses h_{max} and α_{max} can be obtained by using the response STD, skewness and kurtosis through the improved peak factor method in Eq. (4), and the computing formula can be written in $h_{max} = \sigma_h g_{ng,h}$ and $\alpha_{max} = \sigma_\alpha g_{ng,\alpha}$. As response STD, the amplification coefficients of extreme responses are defined as $h_{max}/h_{\max,0}$ and $\alpha_{max}/\alpha_{\max,0}$; moreover, $h_{\max,0}$ and $\alpha_{\max,0}$ are the extreme vertical bending and torsional responses without considering the quadratic terms.

Figs. 11 and 12 show the extreme responses and amplification coefficients respectively. Two aspects are mainly considered with regards to the quadratic term effect: (1) quadratic terms trigger additional excitation STDs and ultimately lead to additional response STDs; and

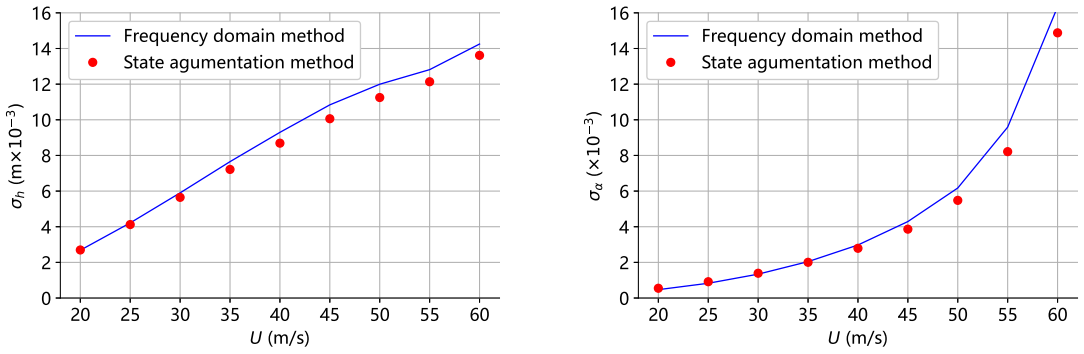

(a) Vertical Response **(b)** Torsional Response

Fig. 6. Comparison of response STD.

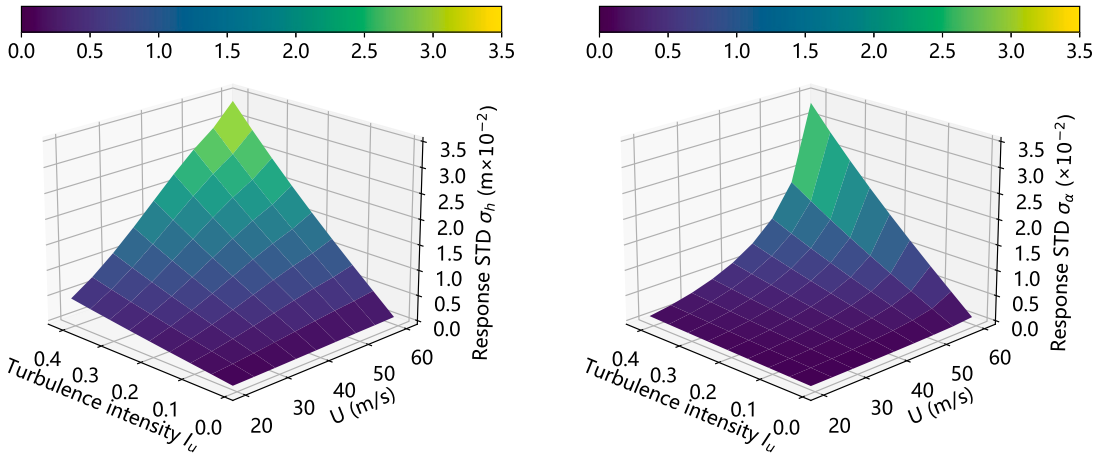

(a) Vertical Response **(b)** Torsional Response

Fig. 7. Response STD.

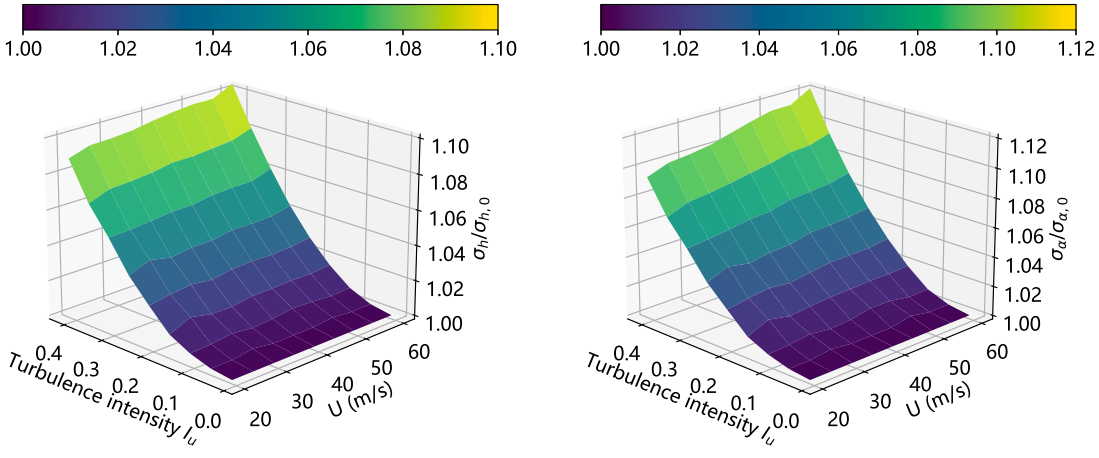

(a) Vertical Response **(b)** Torsional Response

Fig. 8. STD amplification coefficient influenced by nonlinear terms.

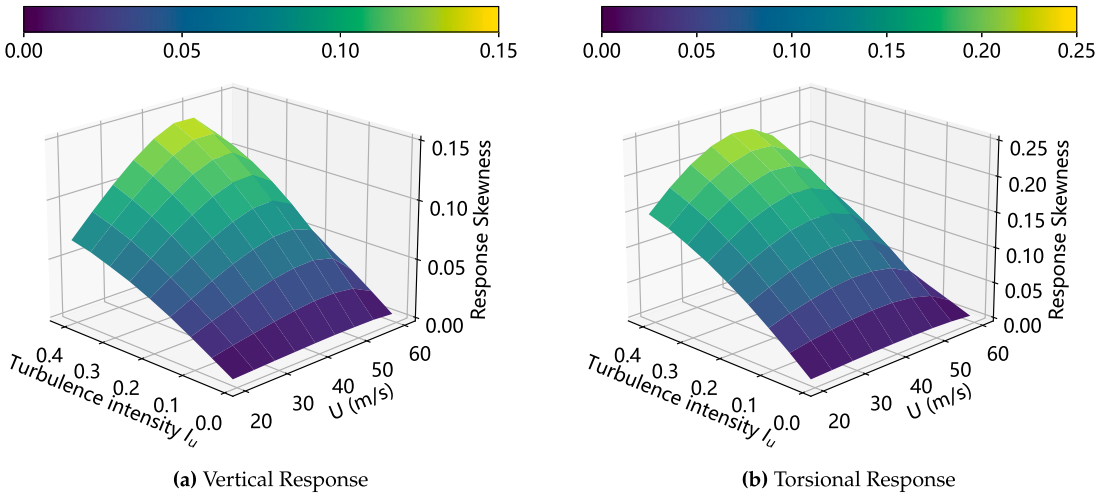

(a) Vertical Response **(b)** Torsional Response

Fig. 9. Response Skewness.

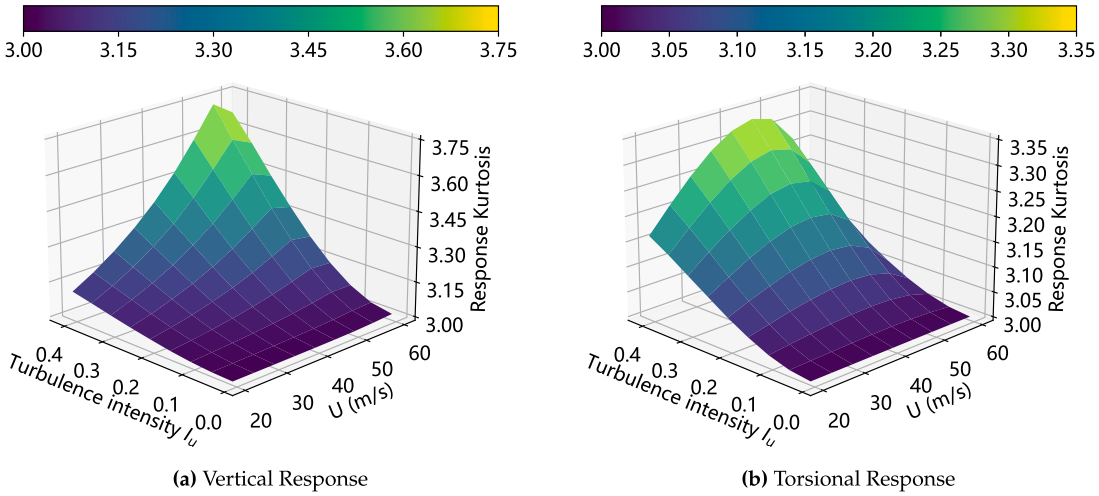

(a) Vertical Response **(b)** Torsional Response

Fig. 10. Response Kurtosis.

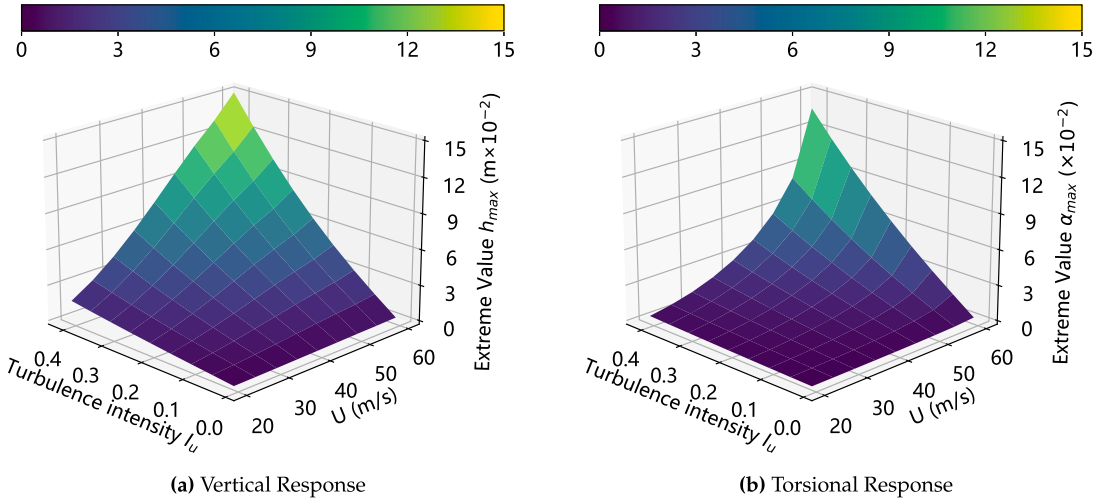

(a) Vertical Response **(b)** Torsional Response

Fig. 11. Extreme responses.

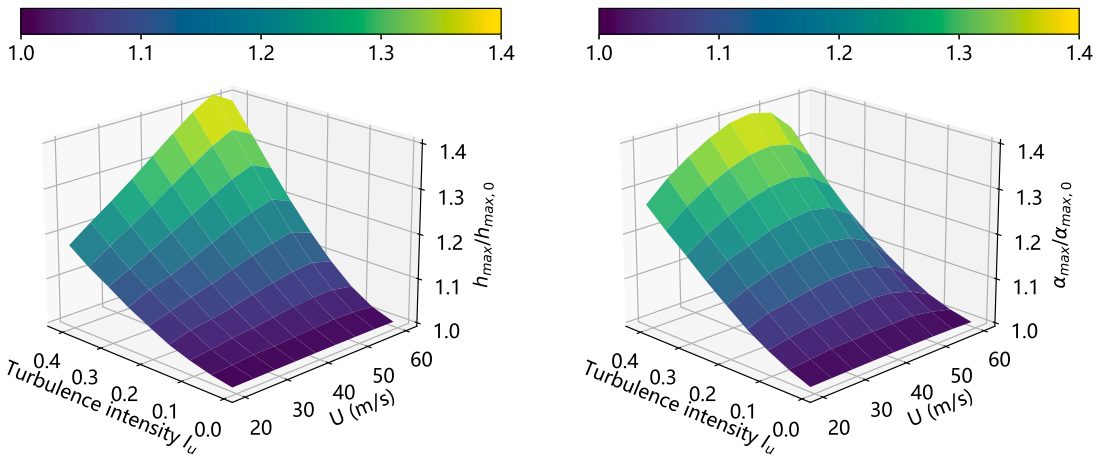

(a) Vertical Response **(b)** Torsional Response

Fig. 12. Amplification coefficient of extreme responses influenced by nonlinear terms.

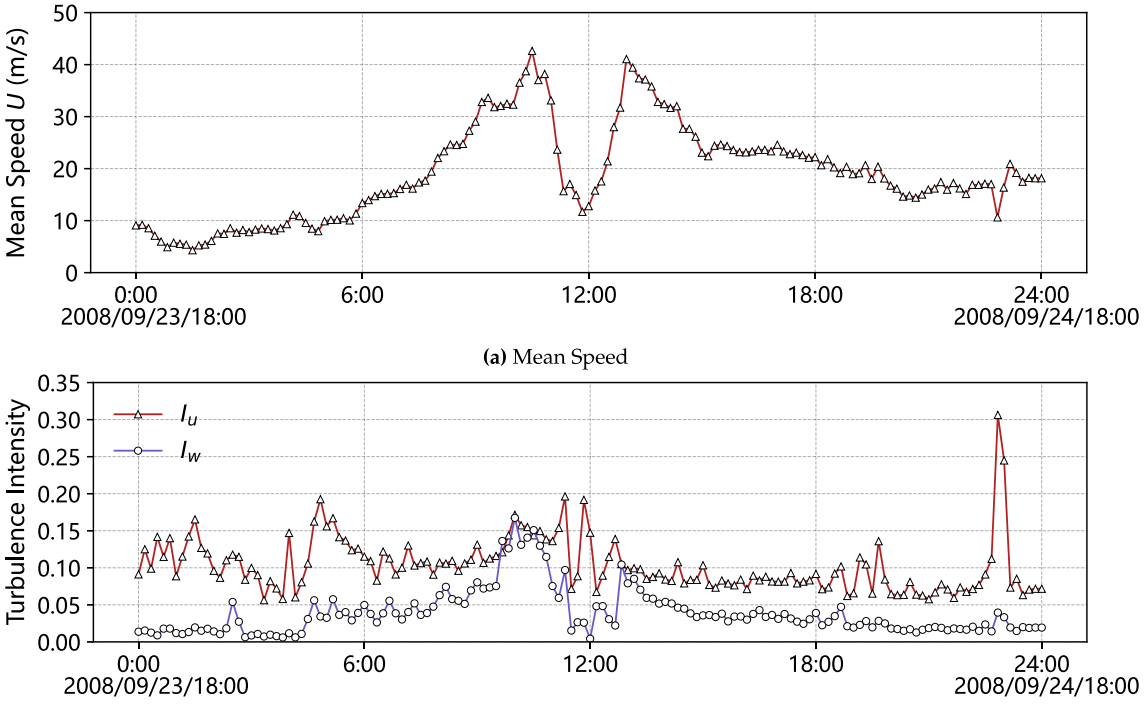

(a) Mean Speed

(b) Turbulence Intensity

Fig. 13. Mean speed and turbulence intensity of Hagupit.

(2) quadratic terms transform the response from a Gaussian random process to a softening process (kurtosis greater than 3), which means the peak factor is larger than that under Gaussian conditions. Under wind climates with large turbulences, the nonlinear buffeting force derived from the geometrical relationship and velocity square terms has an amplification effect on the extreme responses.

5.6. Extreme responses based on typhoon hagupit

More realistically, the bridge buffeting response during typhoon Hagupit is calculated to provide some references for the wind-resistant design of structures. On September 15, 2008, No. 14 Typhoon Hagupit formed over the Northwest Pacific Ocean east of the Philippines, and landed at 6:45 a.m. (Beijing time) on September 24 in the coastal area of Chencun Town, Dianbai County, Guangdong Province, China. The 3-D wind speed time recorded by the observation tower was from 6 p.m. on September 23, 2008 to 6 p.m. on September 24, 2008. Calculated at 10-min intervals, the 24-hour wind speed data can be divided into 144 sets of data, which are used for the analysis and calculation below.

The average wind speed of Hagupit is shown in Fig. 13(a). The wind speed time history shows an 'M' type bimodal distribution. Peak M has a top wind speed of 46 m/s, a bottom wind speed of 11 m/s, and a difference of 35 m/s. During the typhoon, the observation site was always within the strong influence of the typhoon wind field, and

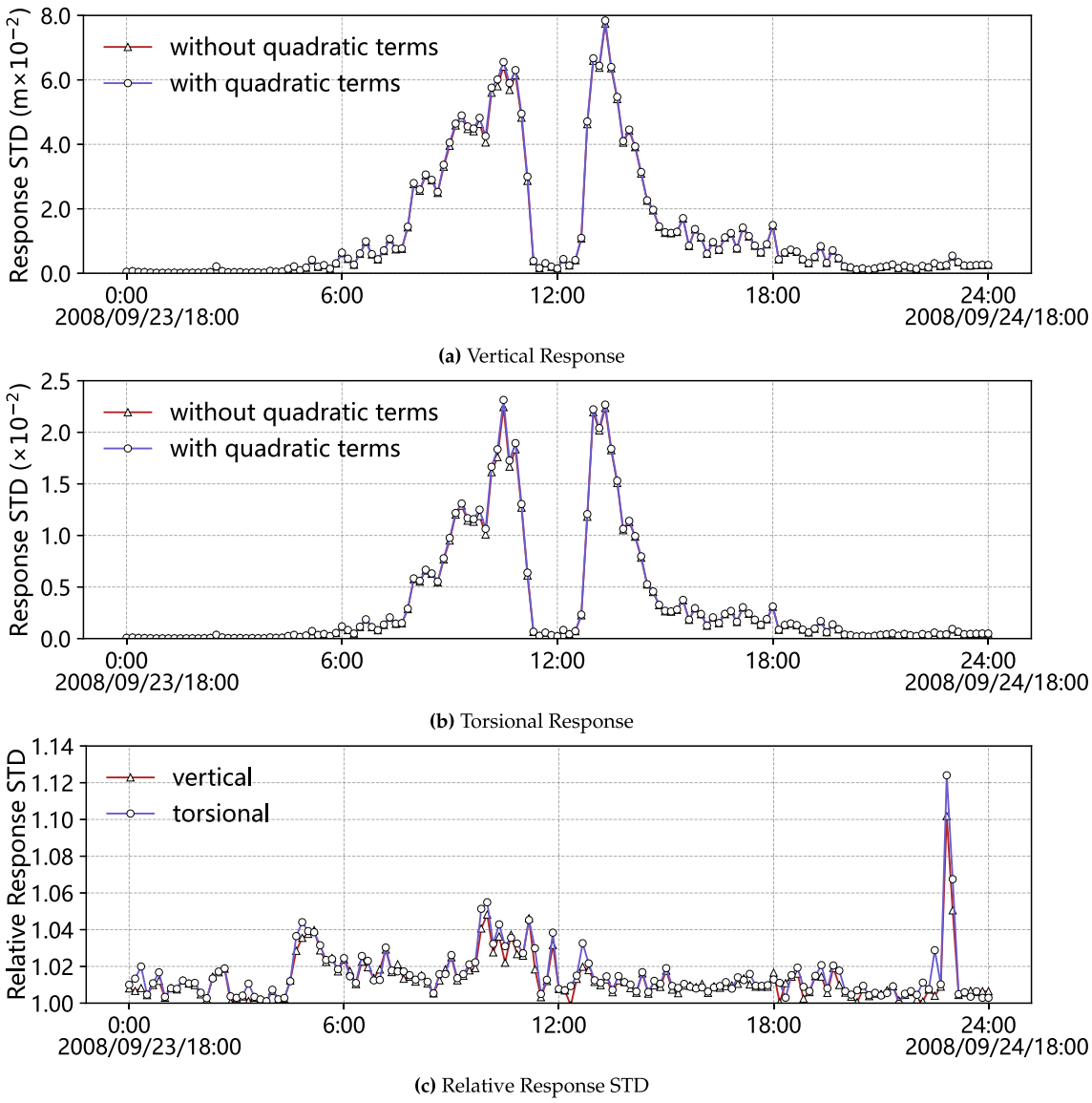

Fig. 14. Response STD under Typhoon Hagupit.

the wind direction before and after the landfall of Hagupit experienced a wind direction change of nearly 180°. The turbulence intensity is shown in Fig. 13(b). The along-wind and vertical turbulence intensity changed dramatically before the landing of Hagupit, and the turbulence intensity was relatively stable after landing. A sudden increase in the turbulence intensity occurred after the typhoon landed.

Figs. 14–17 plot the variations of the response STDs, skewness, kurtosis, peak factors and extreme values sequentially in the whole process of Typhoon Hagupit. As mentioned earlier, it can be obviously found that the nonlinear buffeting force enlarges the extreme value more at these points with a high turbulence intensity, especially at the peak of turbulence intensity at approximately 23:00. However, the wind speed corresponding to this protrusion is quite small, so this point cannot become the most unfavourable working condition for controlling the buffeting response. In contrast, in a short time (10:00 to 11:00 and 1:00 to 2:00) before and after the typhoon eye passed through the bridge site, the turbulence intensity and wind speed reached a large value simultaneously. At this time, the calculated extreme responses are the largest during typhoon landing, and the amplification effect of nonlinear terms is worth considering emphatically.

6. Conclusions

In this paper, the state augmentation method, which is already used to analyse the effect of non-Gaussian turbulence on the buffeting response, is utilized to discuss another non-Gaussianity in the wind loads. This non-Gaussianity comes from velocity quadratic terms in incoming flow and nonlinear geometric relations. First, the non-Gaussian buffeting force is expressed in the polynomials of the OU process. Afterward, the algebraic relationship between the moments of excitation and response is established by Itô's lemma to avoid the low efficiency of the high-order frequency domain method, and the corresponding response STD, skewness and kurtosis are computed from a series of linear moment equations very quickly. Finally, the extreme response is derived from the improved peak factor which considers the non-Gaussian characteristics.

The results show that the amplification of the extreme responses has two parts: the larger response STD generated by the velocity quadratic terms and non-Gaussian peak factors determined by high-order moments. Under the condition of both large turbulence and high wind speed, which often occurs in typhoon climate modes, ignoring

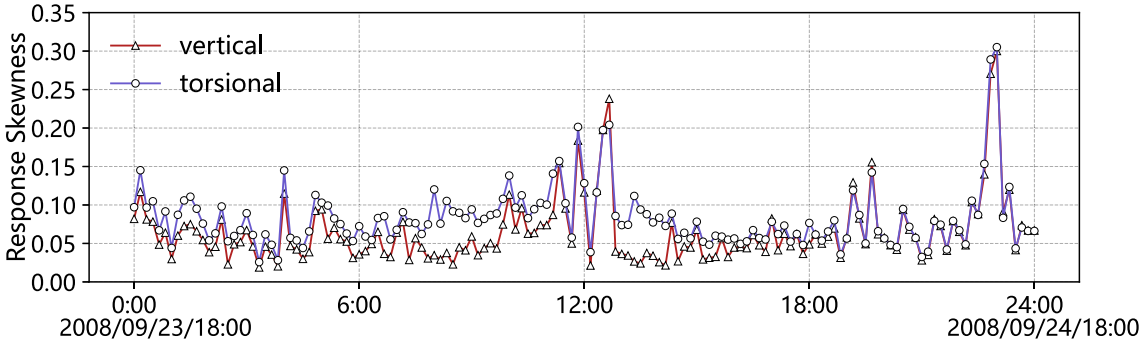

(a) Response Skewness

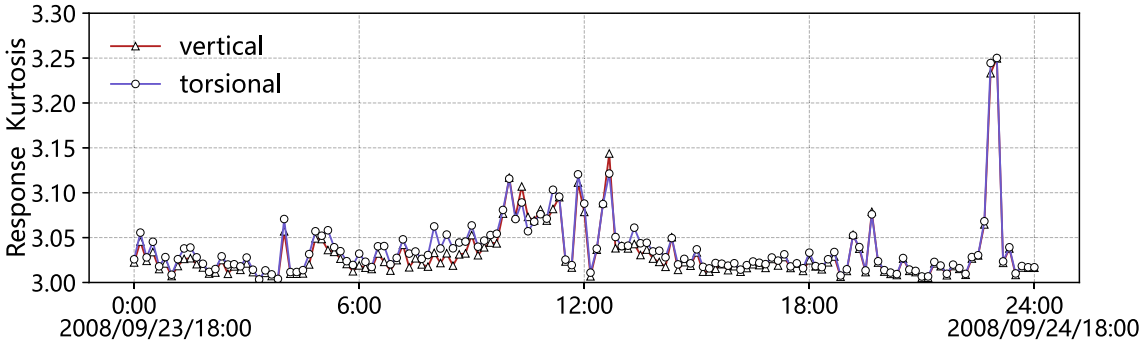

(b) Response Kurtosis

Fig. 15. Response skewness and kurtosis under Typhoon Hagupit.

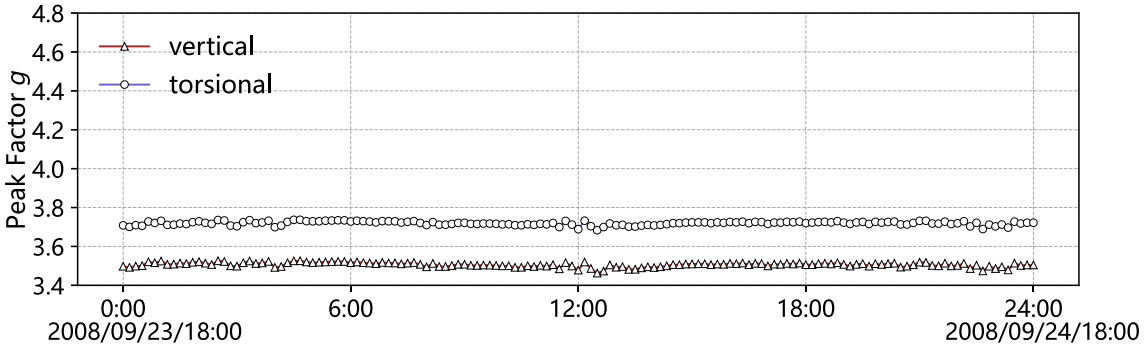

(a) Peak factor for the Gaussian process

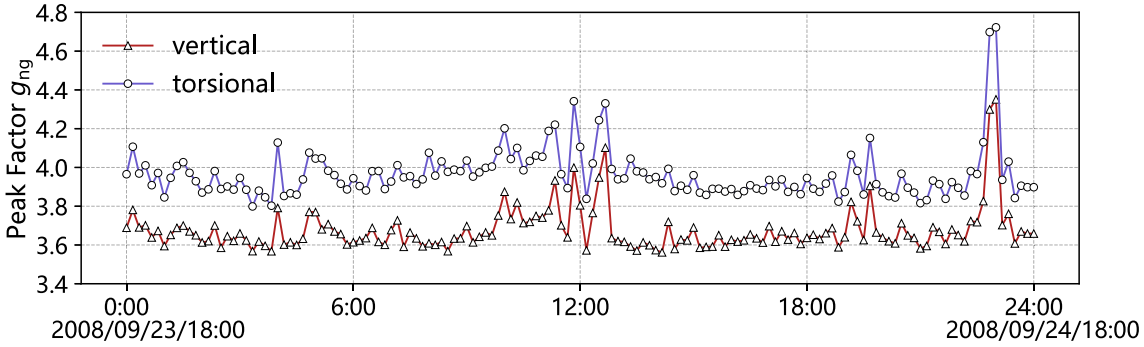

(b) Peak factor for the non-Gaussian process

Fig. 16. Gaussian and non-Gaussian peak factors under Typhoon Hagupit.

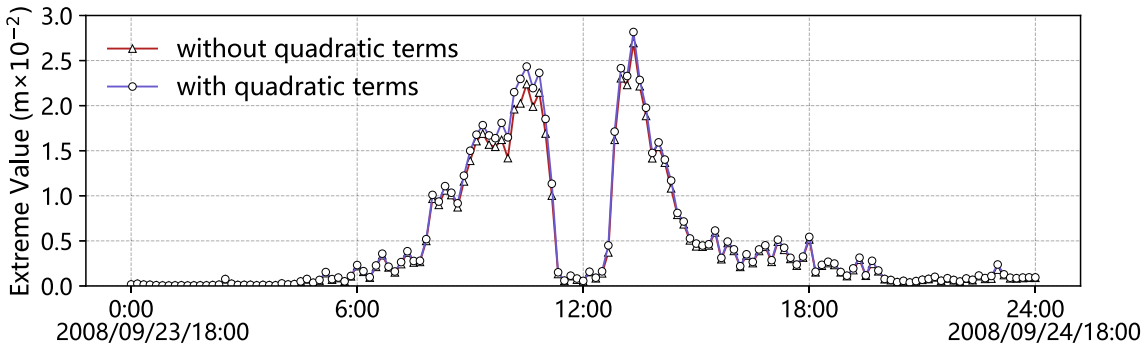

(a) Vertical Response

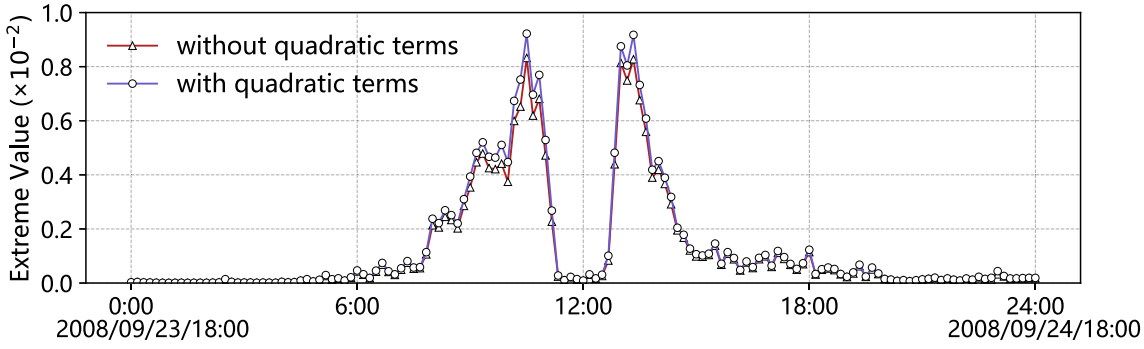

(b) Torsional Response

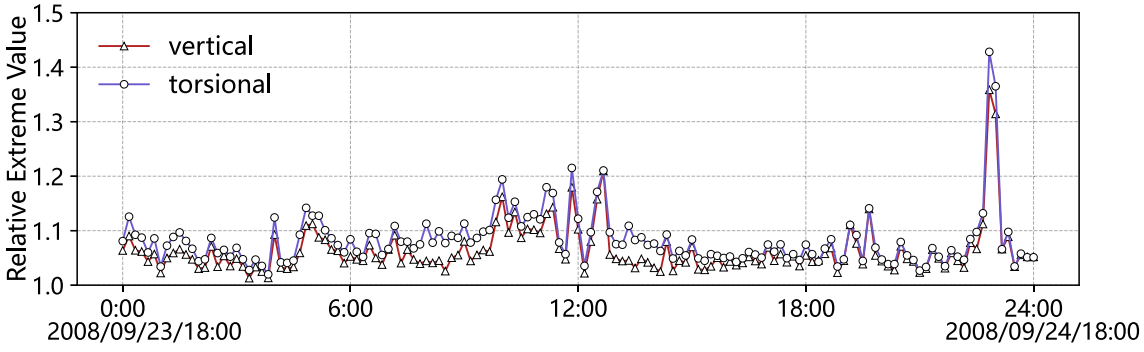

(c) Relative Extreme Response

Fig. 17. Extreme responses under Typhoon Hagupit.

the nonlinear terms may greatly underestimate the extreme responses. However, for long-span bridges with closely spaced natural frequencies, more vibration modes should be systematically taken into moment equations, and the transfer mechanism of non-Gaussianity will be more complex. The moment equation with larger DOF more than 2 should be generated automatically to ensure computational efficiency, which brings difficulty in program implementation. In addition, it is worth noting that aerodynamic admittance based on linear theory can only correct the linear terms u and w rather than the quadratic terms u^2 and w^2. Thus, the above analysis lacks a suitable aerodynamic force model. A more accurate nonlinear buffeting force model for bluff bodies deserves to be investigated carefully by theoretical analysis and wind tunnel experiments, and the influence of nonlinear velocity terms on the structural response needs to be reconsidered.

CRediT authorship contribution statement

Liutian Zhang: Writing – original draft, Conceptualization, Formal analysis, Investigation, Methodology, Validation, Visualization. **Wei Cui:** Methodology, Conceptualization, Supervision, Writing – review & editing, Funding acquisition. **Lin Zhao:** Supervision, Funding acquisition. **Yaojun Ge:** Funding acquisition.

Declaration of competing interest

The authors declare that they have no known competing financial interests or personal relationships that could have appeared to influence the work reported in this paper.

Data availability

Data will be made available on request.

Acknowledgements

The authors gratefully acknowledge the support of the National Key Research and Development Program of China (2021YFF0502200, 2022YFC3005301) and the National Natural Science Foundation of China (52078383, 52008314). Any opinions, findings and conclusions are those of the authors and do not necessarily reflect the reviews of the above agencies.

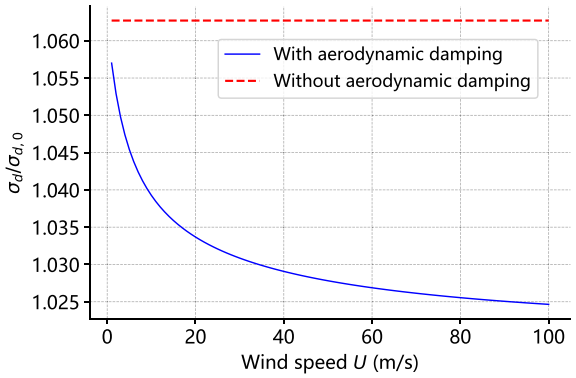

Fig. A.1. STD amplification coefficient of the SDOF tower.

Appendix. The STD amplification factor of the SDOF system

Based on the moment equation in Eq. (18), the STD amplification factor of the SDOF system can be calculated by

$$\begin{aligned}\frac{\sigma_d^2}{\sigma_{d,0}^2} &= \frac{\eta_1 + \frac{1}{4}I_u^2\eta_2 + \eta_3 + \frac{1}{4}I_u^2\eta_4}{\eta_1 + \eta_3}\\ \eta_1 &= \frac{\alpha_1 m_1^2}{c_1(k_1 + \alpha_1^2 m_1 + \alpha_1 c_1)}\\ \eta_2 &= \frac{4\alpha_1 m_1^2}{c_1(k_1 + 4\alpha_1^2 m_1 + 2\alpha_1 c_1)}\\ \eta_3 &= \frac{m_1}{k_1 + \alpha_1^2 m_1 + \alpha_1 c_1}\\ \eta_4 &= \frac{2m_1}{k_1 + 4\alpha_1^2 m_1 + 2\alpha_1 c_1}\end{aligned} \tag{A.1}$$

If the turbulence intensity I_u is fixed, $\sigma_d^2/\sigma_{d,0}^2$ does not change with the wind speed. When aerodynamic damping is taken into consideration, the original damping c_1 should be replaced by $c_1 + \rho A_1 C_D U$. Fig. A.1 plots the amplification factor at different wind speeds, in which $m_1 = 1000$kg, $\xi_0 = 0.03$, $\omega_0 = 0.2\pi$ and $I_u = 0.35$. The amplification factor continuously decreases with wind speed and will approach a certain limit $\sqrt{1 + \frac{1}{4}I_u^2}$.

References

Amirinia, G., Jung, S., 2017. Buffeting response analysis of offshore wind turbines subjected to hurricanes. Ocean Eng. 141, 1–11.

Augusti, G., Borri, C., Marradi, L., Spinelli, P., 1986. On the time-domain analysis of wind response of structures. J. Wind Eng. Ind. Aerodyn. 23, 449–463.

Azzi, Z., Elawady, A., Irwin, P., Chowdhury, A.G., Abi Shdid, C., 2021. Aeroelastic modeling to study the wind-induced response of a self-supported lattice tower. Eng. Struct. 245, 112885.

Benfratello, S., Falsone, G., Muscolino, G., 1996. Influence of the quadratic term in the alongwind stochastic response of SDOF structures. Eng. Struct. 18 (9), 685–695.

Cao, S., Tamura, Y., Kikuchi, N., Saito, M., Nakayama, I., Matsuzaki, Y., 2009. Wind characteristics of a strong typhoon. J. Wind Eng. Ind. Aerodyn. 97 (1), 11–21. http://dx.doi.org/10.1016/j.jweia.2008.10.002, URL https://www.sciencedirect.com/science/article/pii/S016761050800175X.

Chen, X., Kareem, A., 2001. Nonlinear response analysis of long-span bridges under turbulent winds. J. Wind Eng. Ind. Aerodyn. 89 (14–15), 1335–1350.

Chen, X., Matsumoto, M., Kareem, A., 2000. Time domain flutter and buffeting response analysis of bridges. J. Eng. Mech. 126 (1), 7–16.

Cui, W., Caracoglia, L., 2015. Simulation and analysis of intervention costs due to wind-induced damage on tall buildings. Eng. Struct. 87 (15), 183–197.

Cui, W., Caracoglia, L., 2018. A fully-coupled generalized model for multi-directional wind loads on tall buildings: A development of the quasi-steady theory. J. Fluids Struct. 78, 52–68.

Cui, W., Zhao, L., Ge, Y., 2021. Non-Gaussian turbulence induced buffeting responses of long-span bridges. J. Bridge Eng. 26 (8), 04021057.

Cui, W., Zhao, L., Ge, Y., 2022. Non-Gaussian turbulence induced buffeting responses of long-span bridges based on state augmentation method. Eng. Struct. 254.

Davenport, A.G., 1962. Buffeting of suspension bridge by storm winds. J. Struct. Div. 88 (3), 233–268.

Davenport, A.G., 1964. Note on the distribution of the largest value of a random function with applications to gust loading. Proc. Inst. Civ. Eng. 28 (2), 187–196.

Denoël, V., Degée, H., 2006a. Influence of the non-linearity of the aerodynamic coefficients on the skewness of the buffeting drag force. Wind Struct. 9 (6), 457–471.

Denoël, V., Degée, H., 2006b. A simplified method to account for the non linearity of aerodynamic coefficients in the analysis of wind-loaded bridges.

Deodatis, G., 1996. Simulation of ergodic multivariate stochastic processes. J. Eng. Mech. 122 (8), 778–787.

Di Paola, M., Falsone, G., 1997. Higher order statistics of the response of MDOF linear systems under polynomials of filtered normal white noises. Probab. Eng. Mech. 12 (3), 189–196. http://dx.doi.org/10.1016/S0266-8920(96)00038-0, URL https://www.sciencedirect.com/science/article/pii/S0266892096000380.

Fan, W., Sheng, X., Li, Z., Sun, Y., 2022. The higher-order analysis method of statistics analysis for response of linear structure under stationary non-Gaussian excitation. Mech. Syst. Signal Process. 166, 108430.

Fenerci, A., Oiseth, O., 2018. Strong wind characteristics and dynamic response of a long-span suspension bridge during a storm. J. Wind Eng. Ind. Aerodyn. 172, 116–138.

Gong, K., Chen, X., 2014. Influence of non-Gaussian wind characteristics on wind turbine extreme response. Eng. Struct. 59, 727–744. http://dx.doi.org/10.1016/j.engstruct.2013.11.029, URL https://www.sciencedirect.com/science/article/pii/S014102961300583X.

Grigoriu, M., 1984. Crossings of non-Gaussian translation processes. J. Eng. Mech. 110 (4), 610–620.

Grigoriu, M., 2002. Stochastic Calculus: Applications in Science and Engineering. Boston, MA, USA.

Grigoriu, M., Ariaratnam, S.T., 1988. Response of linear systems to polynomials of Gaussian processes. J. Appl. Mech. 55 (4), 905–910.

Gurley, K.R., Tognarelli, M.A., Kareem, A., 1997. Analysis and simulation tools for wind engineering. Probab. Eng. Mech. 12 (1), 9–31.

Gusella, V., Materazzi, A.L., 2000. Non-Gaussian along-wind response analysis in time and frequency domains. Eng. Struct. 22 (1), 49–57.

Jain, A., Jones, N.P., Scanlan, R.H., 1996. Coupled aeroelastic and aerodynamic response analysis of long-span bridges. J. Wind Eng. Ind. Aerodyn. J. Int. Assoc. Wind Eng. 3 (1).

Kareem, A., Tognarelli, M.A., Gurley, K.R., 1998. Modeling and analysis of quadratic term in the wind effects on structures. Eng. Struct. 74 (2), 1101–1110.

Kareem, A., Zhao, J., 1994. Analysis of non-Gaussian surge response of tension leg platforms under wind loads. J. Offshore Mech. Arctic Eng. 116 (3), 137–144.

Karlin, S., Taylor, H.M., 1981. A Second Course in Stochastic Processes. Academic Press, New York, USA.

Kotulski, Z., Sobczyk, K., 1981. Linear systems and normality. J. Stat. Phys. 24, 359–373.

Li, L., Kareem, A., Xiao, Y., Song, L., Zhou, C., 2015. A comparative study of field measurements of the turbulence characteristics of typhoon and hurricane winds. J. Wind Eng. Ind. Aerodyn. 140, 49–66. http://dx.doi.org/10.1016/j.jweia.2014.12.008, URL https://www.sciencedirect.com/science/article/pii/S0167610514002669.

Liu, P., Zhao, L., Fang, G., Ge, Y., 2021. Explicit polynomial regression models of wind characteristics and structural effects on a long-span bridge utilizing onsite monitoring data. Struct. Control Health Monit. 28 (5).

Papadimitriou, C., 1995. Stochastic response cumulants of MDOF linear systems. J. Eng. Mech. 121 (11), 1181–1192. http://dx.doi.org/10.1061/(ASCE)0733-9399(1995)121:11(1181), URL https://ascelibrary.org/doi/abs/10.1061/%28ASCE%290733-9399%281995%29121%3A11%281181%29.

Scanlan, R.H., 1978. The action of flexible bridges under wind, II: Buffeting theory. J. Sound Vibr. 60 (2), 201–211.

Scanlan, R.H., Jones, N.P., 1990. Aeroelastic analysis of cable-stayed bridges. J. Struct. Eng. 116 (2), 279–297.

Soize, C., 1978. Gust loading factors with nonlinear pressure terms. J. Struct. Div. 104 (12), 1937.

Theodorsen, T., 1935. General theory of aerodynamic instability and the mechanism of flutter.

Winerstein, S.R., 1988. Nonlinear vibration models for extremes and fatigue. J. Eng. Mech. 114 (10), 1772–1790.

Xu, Z., Dai, G., Chen, Y.F., Rao, H., 2022a. Prediction of long-term extreme response due to non-Gaussian wind on a HSR cable-stayed bridge by a hybrid approach. J. Wind Eng. Ind. Aerodyn. 231, 105217.

Xu, Z., Dai, G., Zhang, L., Chen, Y.F., Flay, R.G., Rao, H., 2022b. Effect of non-Gaussian turbulence on extreme buffeting response of a high-speed railway sea-crossing bridge. J. Wind Eng. Ind. Aerodyn. 224, 104981.

Yang, L., Gurley, K.R., 2015. Efficient stationary multivariate non-Gaussian simulation based on a Hermite PDF model. Probab. Eng. Mech. 42, 31–41.